Structures of a protein and a virus like particle exhibiting hyperthermo-stability

A Doctoral Thesis

by

Hideaki Tanaka

Submitted to the Graduate School

of Science, Osaka University

Japan

August, 2001

Structures of a protein and a virus like particle exhibiting hyperthermo-stability

A Doctoral Thesis

by

Hideaki Tanaka

Submitted to the Graduate School

of Science, Osaka University

Japan

August, 2001

Acknowledgments

This present work has been carried out under the guidance of Professor Tomitake TSUKIHARA of Institute for Protein Research, Osaka University. I would like to thank him for his incessant guidance and encouragement throughout this work. I am deeply grateful to Associate Professor Katsuhide Yutani for his incessant guidance. I am deeply indebted to Associate Professor Yukio MORIMOTO, Himeji Institute of Technology, and Associate Professor Atsushi NAKAGAWA of Institute for Protein Research, Osaka University, for their helpful suggestion.

I am deeply indebted to Messrs. Tatsuto YAMASHITA, Yoshiyuki KAWAUCHI and Nobuhisa AIBA. I would like to express my deepest appreciation to them.

I am deeply grateful to Drs. Eiki YAMASHITA and Tsunehiro MIZUSHIMA, Institute for Protein Research, Osaka University and Dr. Satoshi Murakami, of Scientific and Industrial Research, Osaka University, for their technical support and helpful advice.

I am also grateful to Drs. Chong Khoon Tee and Naohiro MATSUGAKI of Institute for Protein Research, Osaka University, for their technical support.

I am deeply indebted to Drs. Hiroshi AOYAMA and Takashi Matsumoto, Institute of Physical and Chemical Research and Dr. Takashi TOMIZAKI, Swiss Synchrotron Light Source for their useful help. I am deeply grateful to Dr. Takao SATO of Tokyo Institute of Technology for his valuable suggestion.

I also wish sincere thanks to Associate Professor Yoshiki MATSUURA, Associate Professor Masami Kusunoki and Dr. Genji KURISU of Institute for Protein Research, Osaka University, and Professor Akihito YAMAGUCHI of Institute of Scientific and Industrial Research, Osaka University.

I am deeply grateful to Dr. Masahiro URITANI, Shizuoka University, for his valuable suggestion on ribosome purification. I am deeply indebted to Professor Masanao MICHINOMAE, Konan University, for his useful help and discussion in electron microscopy study. I am also grateful to Dr. Yoshizumi ISHINO, Biomolecular Engineering Research Institute, for his technical advice on culture of *Pyrococcus furiosus*. I am also grateful to Drs. Minoru TOMITA, Shinya IWATA and Ryouichi ICHIKAWA of Tokushima Prefectural Industrial Technology Center, for their technical advice in culture of yeast.

I express my thanks to all members in Tsukihara's laboratories for kind assistance and encouragement. Especially, I express my deepest thanks to Mrs. Yumiko HARA, Misses Akiko TAKAMOTO and Yoko ONO for their useful help in crystallization.

Finally, I thank my parents for their incessant understanding and encouragement.

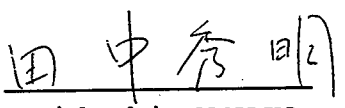

Hideaki TANAKA

August, 2001

TABLE OF CONTENTS

Abbreviations used in this thesis are described as follows :

2-D	2-dimension
ASA	accessible surface area
Abs.	Absorbance
BL	Beam line
Ba	*Bacillus amyloliquefaciens*
*Ba*PCP	PCP from *Bacillus amyloliquefaciens*
DDS	Drug Delivery System
DNA	Deoxiribonucleic acid
DSC	Differential Scanning Calorimetry
DTE	Dithioerythritol
DTT	Dithiothreitol
E. coli	*Eschenrichia coli*
EDTA	Ethylenediaminetetraacetic acid
HEPES	2-[4-(2-hydroxyethyl)-1-piperazinyl]ethanesulfonic acid
IP	Imaging plate
MES	2-morpholinoethanesulfonic acid
MIR	Multiple isomorphous replacement
MIRAS	Multiple isomorphous replacement coupled with anomalous scattering
MPD	2-methyl-2,4-pentanediol

mRNA	Messenger ribonucleic acid
NCS	non-crystallographic symmetry
OD	Optical density
P. furiosus.or Pf	*Pyrococcus furiosus*
PCP	Pyrrolidone carboxyl peptidase
PEG	Polyethylene glycol
*Pf*C142/188S	Cys-free mutant of PCP from *Pyrococcus furiosus*
*Pf*PCP	PCP from *Pyrococcus furiosus*
poly(U)	Polyuridylic acid
rms	root-mean-square
RNA	Ribonucleic acid
RNase	Ribonuclease
rRNA	Ribosomal ribonucleic acid
SDS-PAGE	Sodium dodecyl sulfate polyacrylamide gel electrophoresis
SPMP	Stability Profiles of Mutant Proteins
SPring-8	Super Photon Ring-8
Tl	*Thermococcus litoralis*
*Tl*PCP	PCP from *Thermococcus litoralis*
tRNA	Transfer ribonucleic acid
Tris	Tris(hydroxymethyl)aminomehtane
Triton X-100	Polyoxyethylene (10) octylphenylethter

Chapter 1

Introduction

The conformation of water soluble proteins from mesophiles is marginally maintained by the combination of many positive (such as hydrogen bonds and hydrophobic interaction) and negative (such as entropic factors and steric hindrance) factors for stabilization (Pace et al., 1996). Studies on extremely thermostable proteins from hyperthermophiles that have a denaturation temperature higher than 100 °C would be expected to help us to understand the stabilization mechanism of a general globular protein. Recently, X-ray structures of many proteins from hyperthermophiles have been determined and several factors responsible for extremely thermostable proteins have been proposed, which are increase in the number of ion-pairs and hydrogen bonds (Tanner, et al., 1996; Aguilar et al, 1997; Henning et al., 1995; Henning et al., 1997; Knapp et al., 1997; Korndorfer et al, 1995; Russell et al, 1997; Yip et al, 1995; Tahirov et al., 1998; Yamagata et al., 2001), increase in core hydrophobicity (Spassov et al, 1995; Schumann et al., 1993), decreases in the length of surface loops and peptide chains (Russell et al., 1994; Yamagata et al., 2001), increase in packing

density (Russell et al., 1994; Britton et al., 1995), and the oligomerization of several subunits (Jaenicke et al., 1996, 1998; Sterner et al, 1996; Villeret et al, 1998; Hess et al., 1995; Dams and Jaenicke1999). However, the origin of extremely high thermostabiilty at the molecular level has not yet been elucidated. This might be caused by the fact that the stability results in the offset of many factors and that the contribution of each factor to stability cannot yet be quantitatively estimated.

The pyrrolidone carboxyl peptidase (E.C. 3.4.19.3) (*Pf*PCP) from a hyperthermophilic archaeon, *Pyrococcus furiosus*, which is an enzyme that removes amino-terminal L-pyroglutamic acid from peptides and proteins, is a suitable protein for physicochemically exploring the stabilization mechanism of hyperthermophile proteins, because the thermal denaturation of *Pf*PCP is completely reversible under some conditions and can be thermodynamically analyzed (Ogasahara et al., 1998; Ogasahara et al., 2001). In the case of hyperthermophile proteins, the thermal denaturation is generally irreversible and only a few small proteins are reported to be reversibly denatured (Knapp, 1996; McCrary, 1996). In order to elucidate the mechanism of thermal stability of *Pf*PCP, its three-dimensional structure is needed. I

then determined the X-ray structure of the protein from *P. furiosus*.

Recently, X-ray structures of pyrrolidone carboxyl peptidase (*Tl*PCP) from the hyperthermophilic archaeon, *Thermococcus litoralis* (Singleton et al., 1999), and (*Ba*PCP) from a mesophile, *Bacillus amyloliquefaciens* (Odagaki et al., 1999), have been reported. From the *Tl*PCP structure, the highly hydrophobic insertion that forms the core of the PCP tetramer and the presence of intersubunit disulphide bonds between Cys190 residues in each subunit seem to be responsible for its stability (Singleton et al., 1999). The Cys190 in the *Tl*PCP corresponds to Cys188 in the *Pf*PCP, but there is no corresponding Cys in the *Ba*PCP. The Cys188 in the *Pf*PCP hardly forms a disulphide bond in solution, but the stability remarkably increases when the Cys188 is oxidized (Ogasahara et al., submitted). This is confirmed by DSC (Differential Scanning Calorimetry) experiments using Cys-free mutant *Pf*PCP (*Pf*C142/188S) (Ogasahara et al., submitted). The Cys-free mutant is very suitable for calorimetry because a Cys residue introduces complexity into the heat capacity curve in DSC.

Therefore, in this study, I determined two X-ray structures of *Pf*PCP at 2.2 Å resolution and its Cys-free

mutant protein (*Pf*C142/188S) at 2.7 Å. The origin of the extremely high stability of proteins from hyperthermophiles will be discussed on the basis of structures of the newly determined *Pf*PCPs, those of *Tl*PCP and *Pf*PCP already reported.

Moreover, crystallization of novel virus from *Pyrococcus furiosus* will be discussed. This hyperthermophilic virus was discovered by chance. I have tried to crystallize the 70S ribosome from *P.furiosus.* to elucidate the detailed mechanism of protein biosynthesis processes on the ribosome. The purification procedure of 70S ribosome from *P. furiosus.* with high purity and high activity was established, and these samples were used for crystallization. Although some crystals were obtained from several conditions, they were not ribosome. Further research showed that component of these crystals was novel virus and its gene was integrated in the *P.furiosus* gene. It is the first virus crystal from hyperthermophiles. The crystal structural analysis of this virus will make remarkable progress of structural studies on thermotolerance of virus.

Chapter 2

X-ray crystal structure of PCP from

2-1 Purification and Crystallization of *Pf*PCP

The wild type *Pf*PCP and its Cys mutant (*Pf* C142/188S) were over-expressed in *E.coli* stain JM109/pPCP3 and JM109/pPCP3022, respectively. They were purified as described previously (Ogasahara *et al.*, 1998). Crystallization experiments were carried out at 25 °C using the hanging-drop vapor diffusion method. The concentrations of both purified proteins were adjusted at 10 mg/ml in 80 mM Na-acetate buffer of pH 4.6 (including 4 mM EDTA and 4 mM DTE in the case of the *Pf*PCP). The crystals of the *Pf*PCP were obtained with a reservoir solution containing 80 mM Na-acetate buffer of pH 4.6 including 4 mM EDTA and 4 mM DTE and 4 %(w/v) PEG 4 K. The crystals of the *Pf*C142/188S mutant were obtained from a reservoir solution containing 80 mM Na-acetate of pH 4.6, 0.5 M ammonium sulfate and 30 %(v/v) MPD.

2-2 X-ray data collection

The X-ray intensity data of *Pf*PCP were collected on

Rigaku R-AXIS IIC imaging plates using graphite-monochromated Cu - K α radiation. Those of the *Pf*C142/188S were measured in Mac Science DIP2030 nickel-filtered double-mirror focused Cu - K α radiation. A Rigaku RU-200 rotating—anode X-ray generator was operated at 40 kV and 100 mA. The crystals of the wild-type and its mutant PCPs diffracted up to 2.2 Å and 2.7 Å resolution, respectively. All the intensity data were processed and integrated by the program DENZO and scaled by the program SCALEPACK (Otwinowski, 1997). Statistics of Data collection are summarized in Table 2-1.

Both crystals, the wild type and its Cys mutant, belong to a space group $P2_1$ with cell dimensions of a = 57.9 Å, b = 105.0 Å, c = 78.5 Å and β = 90.7, and a = 49.0 Å, b = 105.8 Å, c = 105.8 Å and β = 96.2, respectively.

2-3 Structure determination and refinement

The structure of the *Pf*PCP was solved by the molecular replacement (MR) method using the X-PLOR package with the X-ray structure of PCP from *Bacillus amyloliquefaciens* (*BaPCP*, PDB entry No. 1AUG). The initial sigma-a weighted electron density map was then refined by solvent flattening (Wang, B. C., 1985), histogram

Table 2-1. Data collection statistics of the wild-type and Cys-free mutant PCPs

	*Pf*PCP wild type	*Pf* C142/188S
Detector	Raxis II C	DIP2030
Generator	Rigaku RU-200	Rigaku RU-200
Collimator(mm)	0.3	0.3
Wavelength(Å)	1.5418	1.5418
Monochromator	Graphite	Double-millor
Conditions	40 kV, 100 mA	40 kV, 100 mA
Temperature(°C)	20	20
Distance(mm)	100	200
Oscillation angle(°)	1.5	1.5
Observed reflections	169,460(10,354)	118,965 (6,425)
Independent reflections	43,412(4,137)	33,343(3,349)
Resolution(Å)	100-2.2(2.3-2.2)	100-2.5(2.61-2.5)
$I/\sigma(I)$	5.8(2.5)	5.0(2.8)
Averaged redundancy	3.9(2.5)	3.6(1.9)
Completeness(%)	91.5(69.9)	89.9(72.0)
R_{merge}	10.1(31.6)	13.0(21.1)
Space group	$P2_1$	$P2_1$
Cell parameters		
a(Å)	57.9	49.0
b(Å)	105.0	105.8
c(Å)	78.5	105.8
β(°)	90.7	96.2

Figures in parentheses are given for the highest resolution shell.

mapping (Zhang, K. Y. J., 1990), and the non-crystallographic symmetry (NCS) averaging technique (Bricogne, G., 1974 and Schuller D., 1996) using the program DM from the CCP4 site (Collaborative Computational Project, Number 4, 1994). The modified electron density map showed the main chain and most of side chains. The PCP was a homotetramer consisting of four independent monomers related by non - crystallographic 222 symmetry. One molecule was built into the electron density map using the program TURBO-FRODO version 5.5 (Jones, T. A., 1985), and other molecules in the asymmetric unit were generated by the non - crystallographic symmetry (NCS) operation. Because the electron density of the N-terminal and C-terminal loop was not clear, $2F_o$-F_c omit maps were used to built structural models of these regions. Simulated annealing followed by positional and B-factor refinements was carried out using the diffraction data in the resolution range between 10 to 2.2 Å with the program X-PLOR (Brunger et al., 1987). The crystal structure was restrained under NCS operations during the refinements. Bulk-solvent correction (Jiang & Brünger, 1994) was applied in the final round of B-factor refinement using the program CNS (Brunger et al., 1998). The structure of the mutant protein, *Pf*C142/188S was determined by the MR

technique using the tetrameric model of *Pf*PCP obtained. Structure refinement of the mutant PCP was performed by following that of the wild-type one. Refinement statistics of both structures are summarized in Table 2-2. Secondary structures of both PCPs were inspected by the program PROCHECK (Roman et al., 1993). Interatomic contacts with a donor-to-acceptor distance of less than 3.2 Å were assigned as hydrogen bonds. Superposition of two molecules and estimation of r.m.s. deviations between them were performed by the program Biocon.

2-4 Quality of the model

The refinement of the *Pf*PCP was converged to an *R* factor of 19.5 % and an R_{free} of 23.2 % for reflections in the resolution range 10-2.2 Å (R_{free} is calculated using 5 % of reflections). The Cys-free mutant (*Pf*C142/188S) was refined to an *R* factor of 21.0 % and an R_{free} of 24.3 % for the reflections from 10 to 2.7 Å. Both current models include all 832 residues, 208 residues in each of four subunits, and 168 water molecules for *Pf*PCP and 124 water molecules for *Pf*C142/188S. The refined structure model of *Pf*PCP converged well with rms deviations from the ideal bond length and the angles of 0.017 Å and 3.09°,

Table 2-2. Refinement statistics

	*Pf*PCP wild type	*Pf* C142/188S
Resolution(Å)	10-2.2	10-2.7
Reflections used	40718	25840
No. of protein residues	832	832
No. of water molecules	168	124
R factor(%)	19.5	21.0
R_{free}(%)	23.2	24.3
R.m.s.d from ideality		
bond length(Å)	0.017	0.025
bond angles(°)	3.09	3.68
Ramachandran plot statistics		
Residues in most favored region (%)	90.6	89.7
Residues in additionally allowed region (%)	9.2	10.3
Residues in generously allowed region (%)	0.1	0.0
Residues in disallowed region (%)	0.0	0.0
Average B factor		
main chain($Å^2$)	37.9	24.5
side chain($Å^2$)	44.3	29.5

respectively. 90.6 % of the non-glycine residues was in the most favorable region of the Ramachandran plot, 9.2 % in the additionally allowed region and no residues in the disallowed region (Roman et al., 1993). Pro159 in each subunit was in a *cis* conformation. The rms deviations from the ideal bond length and the angles for *Pf*C142/188S were 0.025 Å and 3.68°, respectively. 89.7 % of the non-glycine residues were in the most favorable region of the Ramachandran plot, 10.3 % in the additionally allowed region and no residues in the disallowed region. The final coordinates have been deposited in the Protein Data Bank (accession No. 1IOF and No. 1IOI).

2-5 Monomer structure

The structure of the *Pf*PCP monomer is depicted by a ribbon drawing in Figure 2-1. Monomeric structures of *BaPCP* and *TlPCP* superposed on that of *Pf*PCP by the program O (Jones et al., 1990) were drawn by stereoscopic Cα traces using TRUBO-FRODO (Jones et al., 1985) (Figure 2-2). The *Pf*PCP monomer folded into a single α/β globular domain. The central β-sheet comprised four-strand parallel β sheets (β3, β1, β4 and β9), two short two-strand anti-parallel β sheets (one with β2 and β3, and the other with

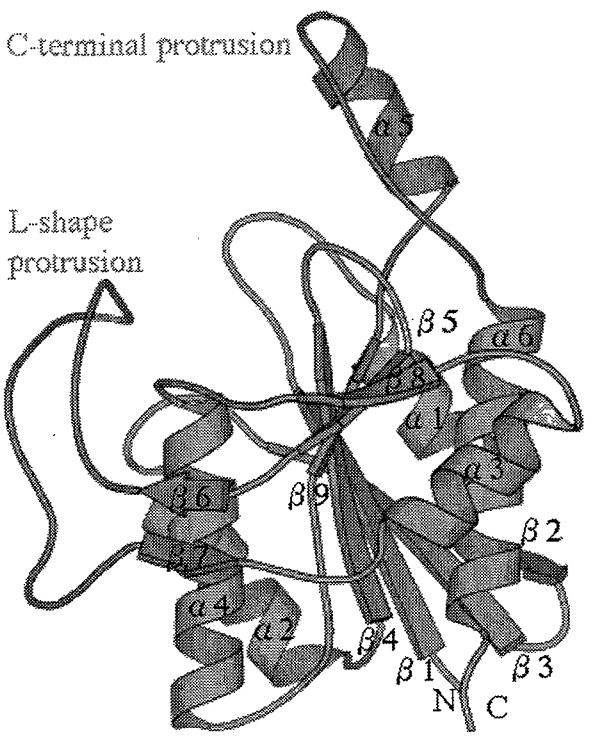

Figure 2-1. A ribon diagram of a *Pf*PCP monomer with the secondary structure elements. This figure was produced with the program MOLSCRIPT (Kraulis, P. J., 1991).

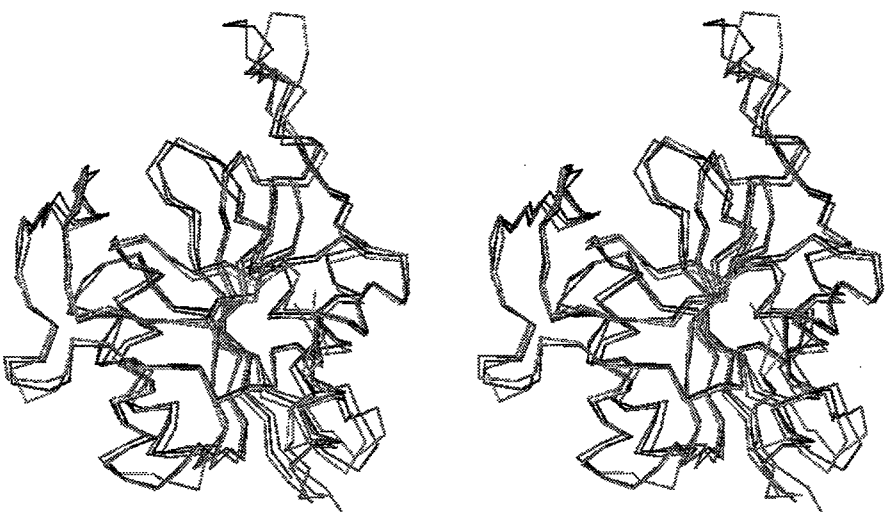

Figure 2-2. Stereo view of three PCP monomers. *BaPCP* : Blue, *TlPCP* : Orange and *PF*PCP : Red. This figure was produced using TURBO-FRODO.

β5 and β9) and a short parallel β-sheet (β5 and β8). The central β-sheet was sandwiched within five α-helices; two helices (α2 and α4) on one side and three helices (α1, α6 and α3) on the other side. Polypeptide segments from Arg80 to Ser113 and from Tyr169 to Cys188 protruded from the core α/β domain, which are termed C-terminal protrusion and L-shape protrusion, respectively, in this paper. The C-terminal protrusion included a 2.5 turn α-helix of α5 and an extended strand. The L-shape protrusion consisted of a short two-strand anti-parallel β-sheet (β6 and β7) at the horizontal line of L and a distorted anti-parallel β-sheet at the vertical line which was assigned to a loop by the program PROCHECK. Both the C-terminal and the L-shape protrusions have higher temperature factors than the core domain.

2-6 Tetramermer structure

*Pf*PCP exhibited a tetrameric structure similar to that of *T1PCP* and *BaPCP*. Individual subunits of *Pf*PCP, termed A, B, C and D, were superposed well on the other subunits related by 222 symmetries within r.m.s. displacements less than 0.023 Å for all the main-chain atoms. Three two-fold axes were designated by P-, Q- and

R-axes as shown in Figure 2-3. The P-axis relates A to C and D to B, the Q-axis, A to D and C to B, and the R-axis, A to B and C to D. Each subunit of *Pf*PCP contacted two other subunits at two different interfaces. One interface through which the P-axis ran was designated the P-interface, and the other around the Q-axis, the Q-interface. The intersubunit contacts in the P-interface were mostly hydrophobic interactions, while those at the Q-interface included ion bonds and hydrophobic interactions.

The hydrophobic contacts between two C-terminal protrusions related by the P-axis were the main intersubunit interaction in the P-interface. Each C-terminal protrusion had an additional intersubunit interaction with a C-terminal end of α3, a loop between an α3 and a β8, a strand of β8, a loop between β4 and β5, and an N-terminal end of α6. Hydrophobic interactions were prominent, and no ion bond was detected at the P-axis interface.

The L-shape protrusion was responsible for the intermolecular interactions at the Q-interface. This protrusion interacted with the equivalent part related by the Q-axis symmetry, an N-terminal end of α2, an N-terminal end of α3, a C-terminal end of β5, a loop between

a) *Pf*PCP

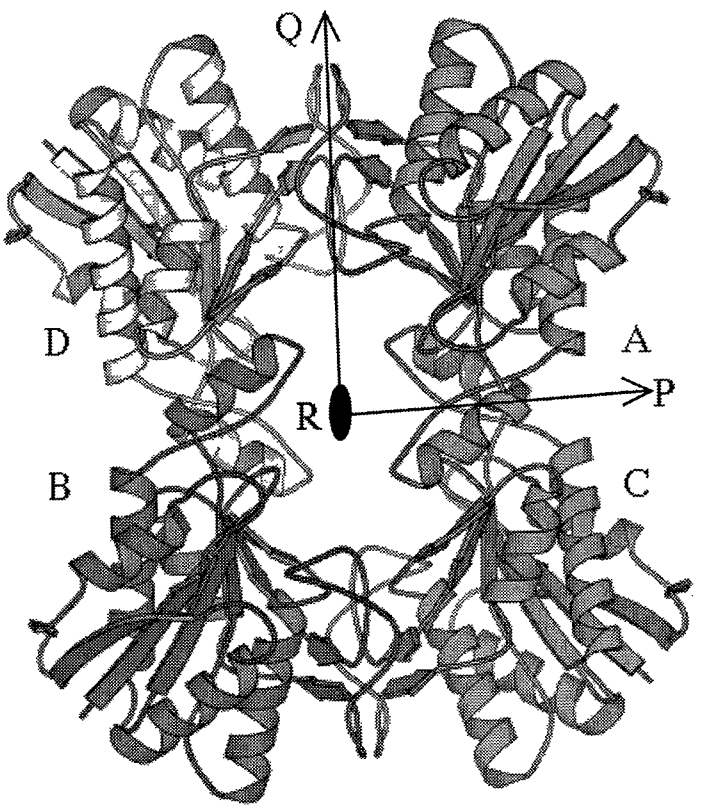

b) *Ba*PCP

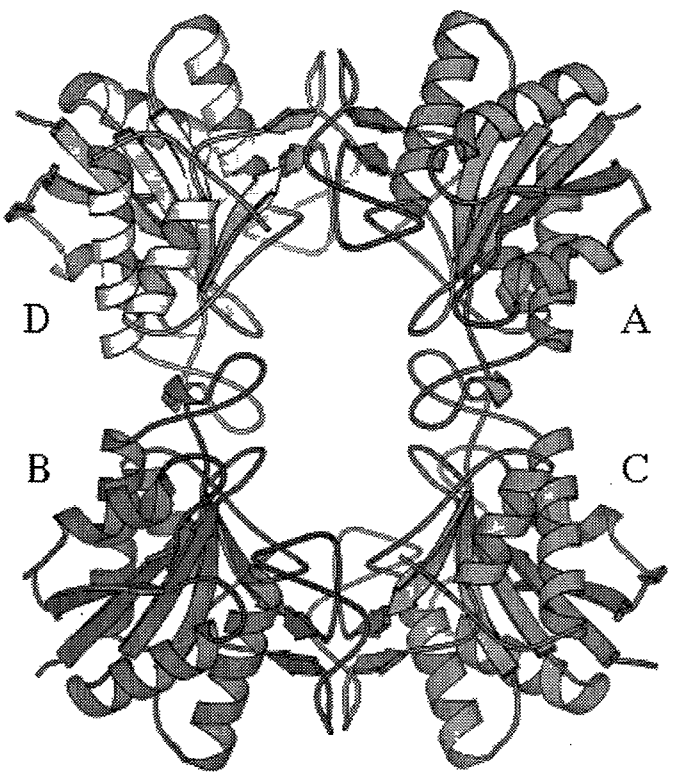

c) *TlPCP*

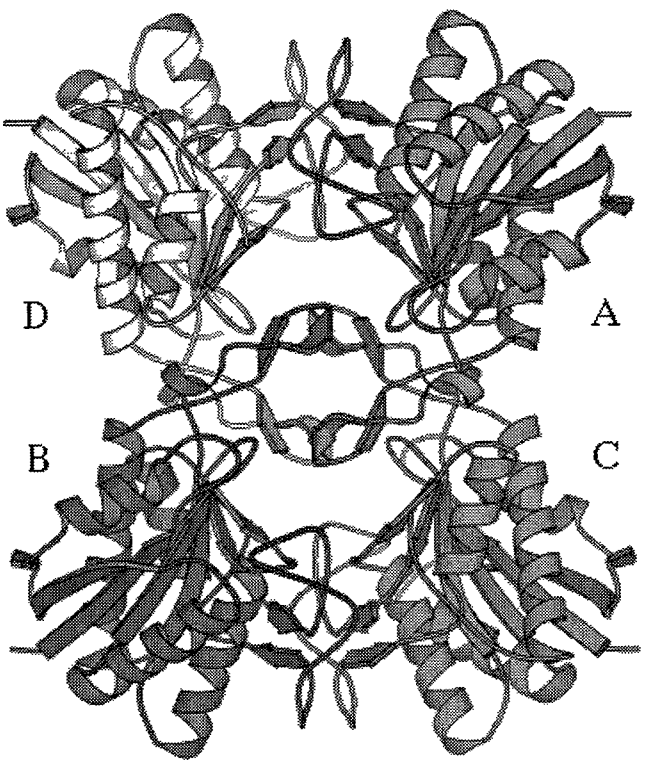

Figure 2-3. Schematic drawing of the structure of *Pf*PCP tetramer. Each monomer is shown in a different color. The figure was produced by using MOLSCRIPT (Kraulis, P. J., 1991).

β5 and β6, a C-terminal end of β8, a loop between β8 and α4, and an N-terminal end of α4. Ten ion bonds were detected at this interface. They were Asp87-Arg80, Asp100-Lys118, Glu99-Lys118, Asp100-Arg80, Asp100-Lys118, and their two-fold symmetry-related pairs. In addition to these charged amino acids, Ile81, Val83, Ala85, Thr109, Ala110, Tyr111, Phe1112, Ser136 and Leu139 were included in hydrophobic interaction around the Q-axis.

In *TlPCP*, Cys190 located close to the end of the C-terminal protrusion, that is, at the beginning of the C-terminal helix (α6) in each monomer, forms disulfide bond (A-C and B-D) (Singleton et al., 1999). Although the *Pf*PCP has Cys188 located at the equivalent position, inter-subunit disulfide bond was not observed as shown in Figure 3. The distance of Cys188 Sγ between A and C was 3.77 Å.

2-7 The active site

The *Pf*PCP has two cysteine residues, Cys142 and Cys188, and one of the cysteine-residues (Cys142) is completely conserved in all known PCP sequences. This conserved residue plays a key role in PCP activity. In *Pf*PCP, a nucleophilic Cys142 was located in the beginning

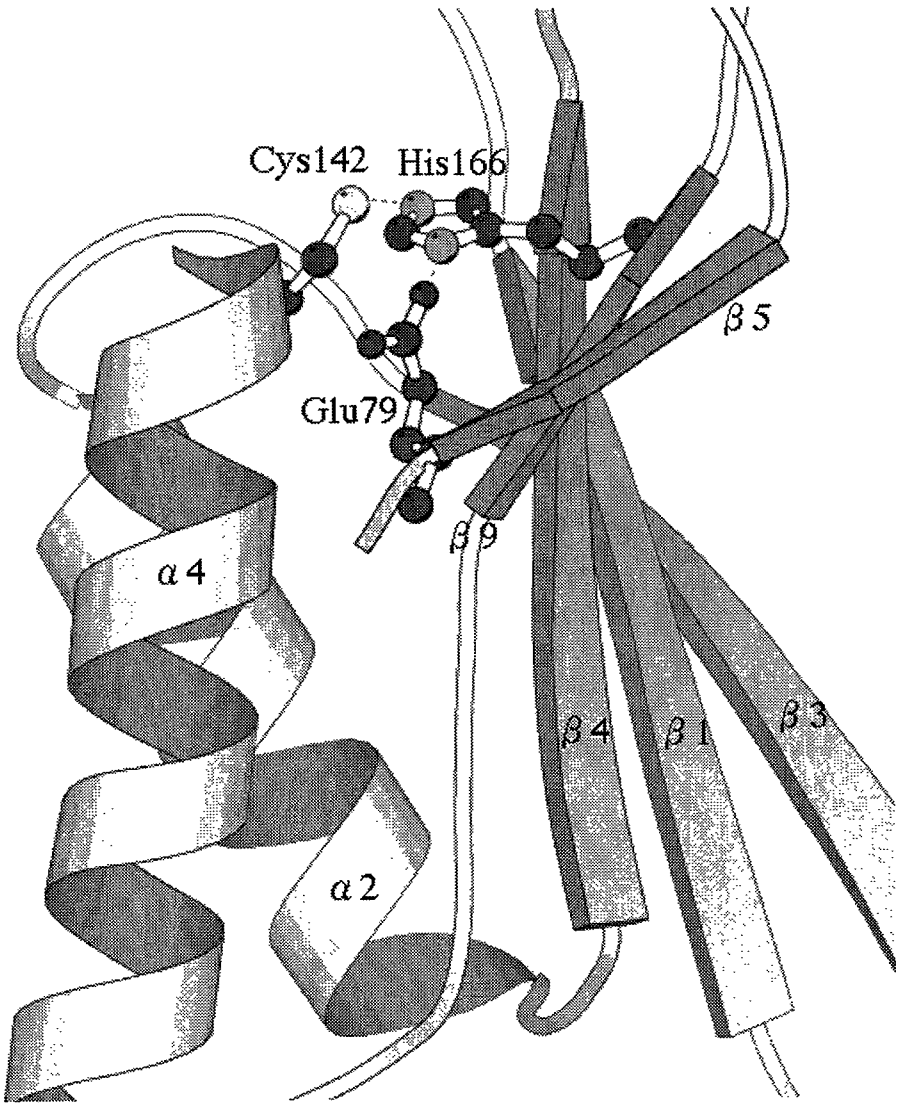

Figure 2-4. Schematic drawing of the *Pf*PCP active site triad Cys142, His166, Glu79. Cys142 Sγ - His166 Nε1 and His166 Nδ - Cys142 Sγ form hydrogen bonds with distances of 3.49 Å and 2.72 Å, respectively. The figure was produced by using MOLSCRIPT (Kraulis, P. J., 1991).

of α4 near the central sheet (β5 and β9). A schematic drawing of the *Pf*PCP active site is shown in Figure 2-4.His166 located in the α9 has also been suggested to be a second component of the Cys-His catalytic dyad. The Cys142 Sγ forms a hydrogen bond to His166 Nε1 with a distance of 3.49 Å. Glu79, the third component of a catalytic triad, was located in the loop between β5 and β6. The Glu79 Oε formed a hydrogen bond to His166 Nδ with a distance of 2.72 Å. The sequence of this catalytic triad, Cys-His-Glu is highly conserved in all known PCP sequences, and its three-dimensional arrangement of *Pf*PCP is consistent with those of other PCP structures.

2-8 Structure of the *Pf* C142/188S

The overall X-ray structure of the Cys-free mutant PCP was essentially identical to that of the wild-type PCP. The r.m.s. deviations for the main chain atoms between *Pf*PCP and *Pf*C142/188S was 0.271 Å. Slight deviations were found as shown in Figure 2-5 restricted in a few flexible loops (β1 - α1, β2-β3, and α5-α6). The intersubunit contact between two Ser 188 Oγ of A and C subunits in *Pf* C142/188S was not detected as that between two Cys 188 Sγ of A and C subunits in *Pf*PCP(Figure 2-6 a and b). This result

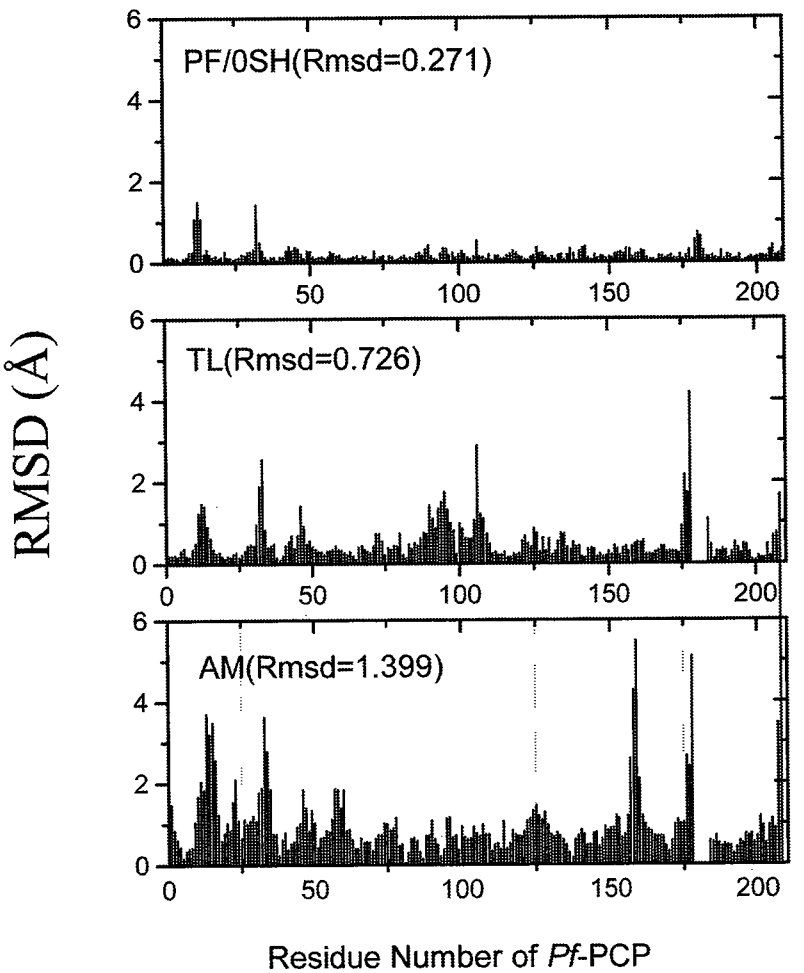

Figure 2-5. Rms deviation of C atoms between *Pf*PCP and *Pf*C142/188S (a), between *åPCP* and *TlPCP* (b), and between *Pf*PCP and *Ba*PCP (c) after a least fit of corresponding C atoms. In the case of (a), all residues (208) were used. In (b) and (c), the corresponding residues to *Pf*PCP (1 to 177 and 184 to 208) were used.

a) *Pf*PCP

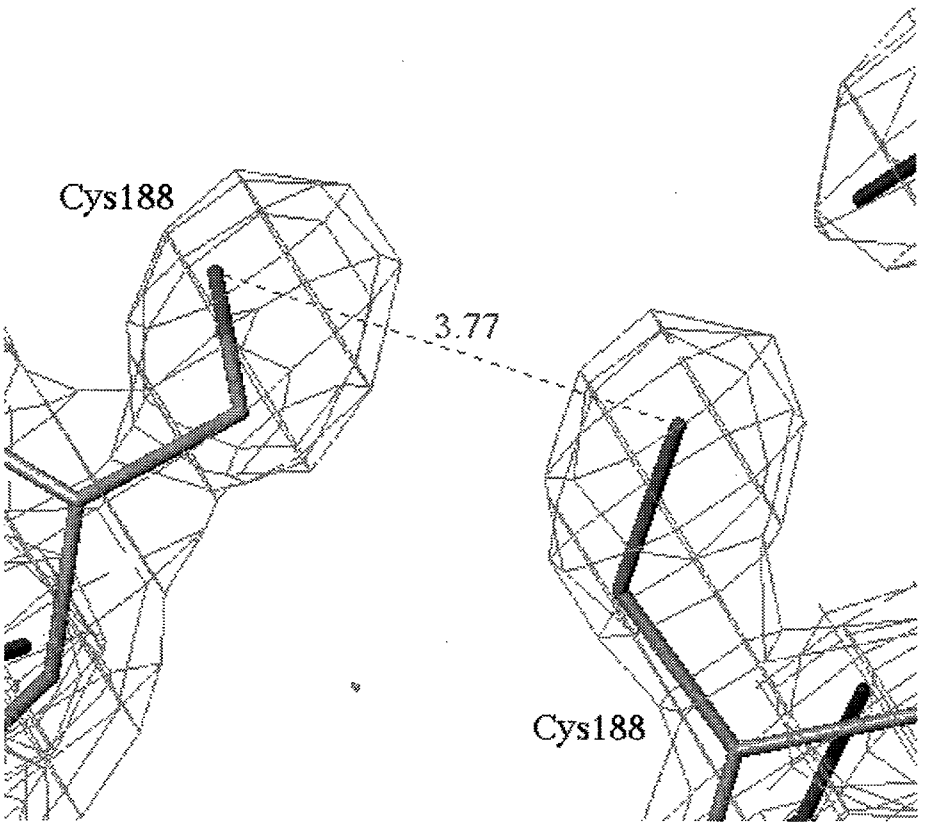

Figure 2-6-a. Cys188 located at the interface of each monomer (A-C and B-D). A $2F_o$-F_c electron density map calculated in the resolution range 10-2.2 Å is shown. The distance of Cys188 Sγ between A and C in *Pf*PCP was 3.77 Å. There is not a disulfide bond between the monomers. This figure was produced using TURBO-FRODO.

b) *Pf* C142/188S

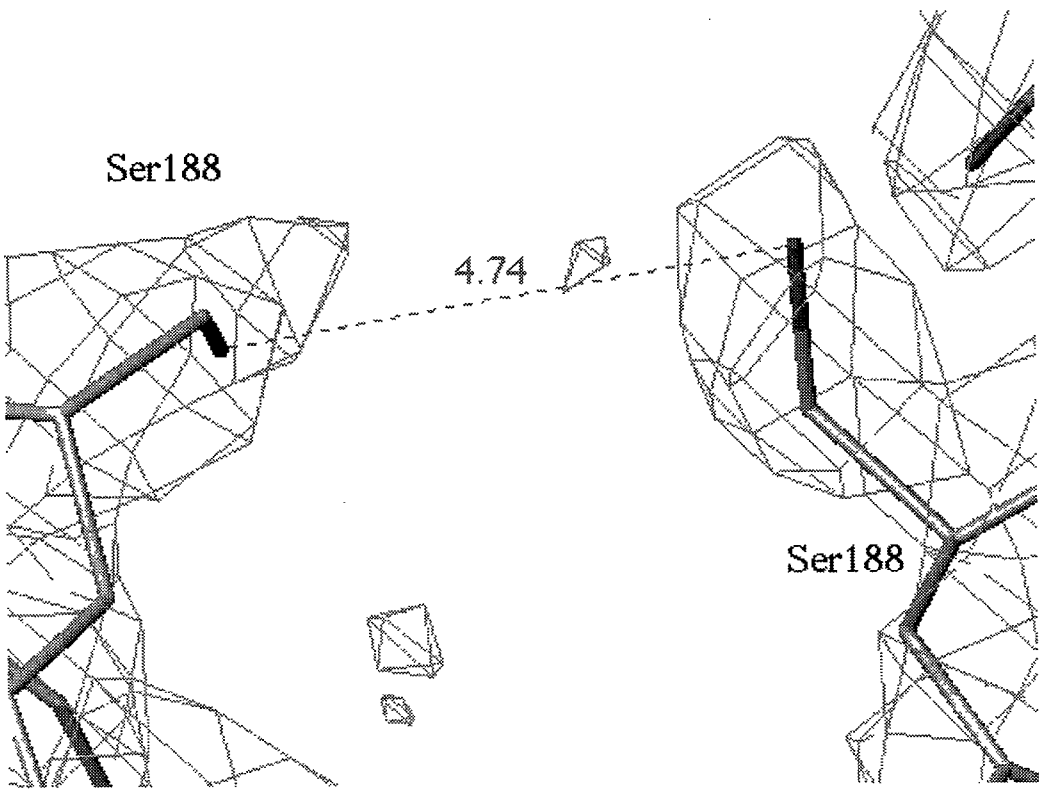

Figure 2-6-b. Ser188 located at the interface of each monomer (A-C and B-D). A $2F_o$-F_c electron density map calculated in the resolution range 10-2.7 Å is shown. The distance of Ser188 Oγ between A and C in *Pf* C142/188S was 4.74 Å. This figure was produced using TURBO-FRODO.

indicates that the Cys mutation hardly perturbs the conformation of the wild type PCP and that *Pf*C142/188S is a very suitable protein for studying the extremely high stability of *Pf*PCP using DSC, because *Pf*C142/188S does not introduce complexity into the heat capacity curve in DSC due to the Cys residues.

2-9 Structural Comparison of Three PCPs

As shown in Figure 2-2, large structural variations were detected in the C-terminal protrusion among three PCPs, where 5 and 6 residues were inserted in *Pf*PCP and *TlPCP*, respectively (Figure 2-7). Excluding the amino acid residues which did not have equivalent residues among the three PCPs, the rms deviations of Cα atoms were evaluated. The deviations of *Pf*PCP to *TlPCP* and *Ba*PCP were 0.726 Å and 1.399 Å, respectively (Figure 2-5). This suggests that *Pf*PCP was closer to *TlPCP* than to *Ba*PCP in the main-chain fold, corresponding to the sequence homology. The sequence alignments of the three PCPs and a schematic drawing of the secondary structure of *Pf*PCP are shown in Figure 2-7. The amino acid sequence of *Pf*PCP had 39.4 % (82/208) identity with that of *Ba*PCP and 56.3 % (117/208) identity with that of *TlPCP* sequence.

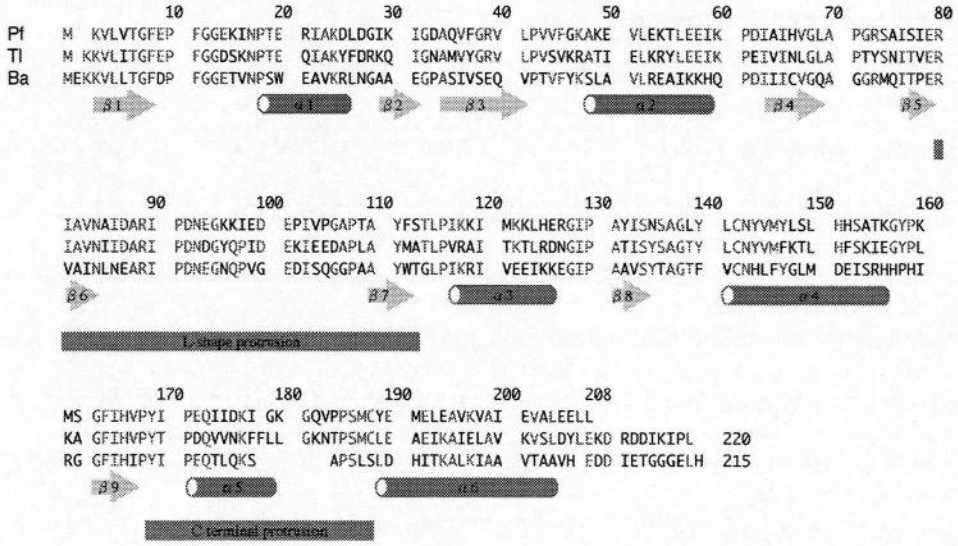

Figure 2-7. The sequence alignments of three PCPs and schematic drawing of the secondary structure of *Pf*PCP. An α - helix and β - strand are shown by a cylinder and a arrow, respectively.

On the other hand, remarkable differences in the structures between *Pf*PCP and *Tl*PCP were detected in six regions along the sequence, which were turns of β1 - α1, β2 - β3 and β3 - α2, as L-shape protrusion, a C-terminal protrusion and a C-terminal coil. The largest conformational change between *Pf*PCP and *Tl*PCP was detected in the C-terminal protrusion as shown in Figure 2-2. This region of *Pf*PCP contacted another subunit at the P-interface, while that of *Tl*PCP interacted with two different subunits at the P- and R-interfaces. The conformational difference in the L-shape protrusion between *Pf*PCP and *Tl*PCP was larger than that between *Pf*PCP and *Ba*PCP. This region of any PCP interacted with another subunit related by the Q-axis symmetry. Large conformational differences between *Pf*PCP and *Ba*PCP were detected in the turns of β1 - α1, β2 - β3, β3 - α2, α2 - β4 and α4 - β9, the C-terminal protrusion and the C-terminal coil. *Pf*PCP had a five-residue insertion compared with *Ba*PCP in the C-terminal protrusion. This insertion affected a remarkable conformational difference in this region.

The number of hydrogen bonds per residue for *Pf*PCP, *Tl*PCP, and *Ba*PCP was 2.13, 2.16 and 2.00, respectively. The two hyperthermophile PCPs had more hydrogen bonds than

Table 2-3. Ion pairs of the three PCPs from different sources within 4 Å.

a) *Pf*PCP

residue	residue		location
14 GLU	177 LYS		c - a5
20 GLU	24 LYS		a1 - a1
27 ASP	39 ARG		a1 - b3
53 GLU	152 HIS		a2 - a4
57 GLU	156 LYS		a2 - a4
62 ASP	2 LYS		b4 - c
62 ASP	160 LYS		b4 - c
79 GLU	73 ARG		b5 - c
79 GLU	166 HIS		b5 - b9
87 ASP	80 ARG	A-D	c - c
87 ASP	118 LYS	A-D	c - a3
99 GLU	97 LYS		c - c
99 GLU	118 LYS	A-D	c - a3
100 ASP	80 ARG	A-D	c - c
100 ASP	118 LYS	A-D	c - a3
172 GLU	21 ARG		a5 - a1
176 ASP	177 LYS		a5 - a5
194 GLU	127 ARG		a6 - c
201 GLU	127 ARG		a6 - c
206 GLU	119 LYS		c - a3

b) *BaPCP*

residue	residue		location
23 GLU	26 LYS		a1 - a1
23 GLU	27 ARG		a1 - a1
33 GLU	194 LYS		c - a6
41 GLU	60 LYS		b2 - a2
41 GLU	61 HIS		b2 - a2
81 GLU	75 ARG		c - c
81 GLU	168 HIS		c - b6
89 GLU	82 ARG	A-D	c - c
89 GLU	120 LYS	A-D	c - a3
96 GLU	49 LYS		c - a2
124 GLU	127 LYS		a3 - a3
129 GLU	191 LYS		c - a6
153 ASP	157 ARG		a4 - a4
154 GLU	55 ARG		a4 - a2
154 GLU	157 ARG		a4 - a4
154 GLU	158 HIS		a4 - c
154 GLU	159 HIS		a4 - c
204 GLU	163 ARG		c - b6
205 ASP	121 ARG		c - a3

c) *T1PCP*

residue	residue	location	
15 ASP	178 LYS		c - c
21 GLU	25 LYS		a1 - a1
28 ASP	40 ARG		c - b3
58 GLU	54 LYS		a2 - a2
59 GLU	55 ARG		a2 - a2
80 GLU	167 HIS		c - b9
88 ASP	119 ARG	A-D	c - a3
95 ASP	48 ARG		c - a2
101 ASP	81 ARG	A-D	c - c
101 ASP	119 ARG	A-D	c - a3
105 GLU	152 HIS		c - a4
127 ASP	123 LYS		a3 - a3
199 GLU	196 LYS		a6 - a6
199 GLU	203 LYS		a6 - a6
207 ASP	213 ARG		a6 - c
210 GLU	2 LYS		a6 - c

A-D represents an inter-subunit ion pair between Subunit A and D. Others an intra-subunit ion pair in Subunit A. The last row in each PCP shows the location of ion pairs (α; α-helix, β; β-sheet, c; coil or turn).

a) *Pf*PCP

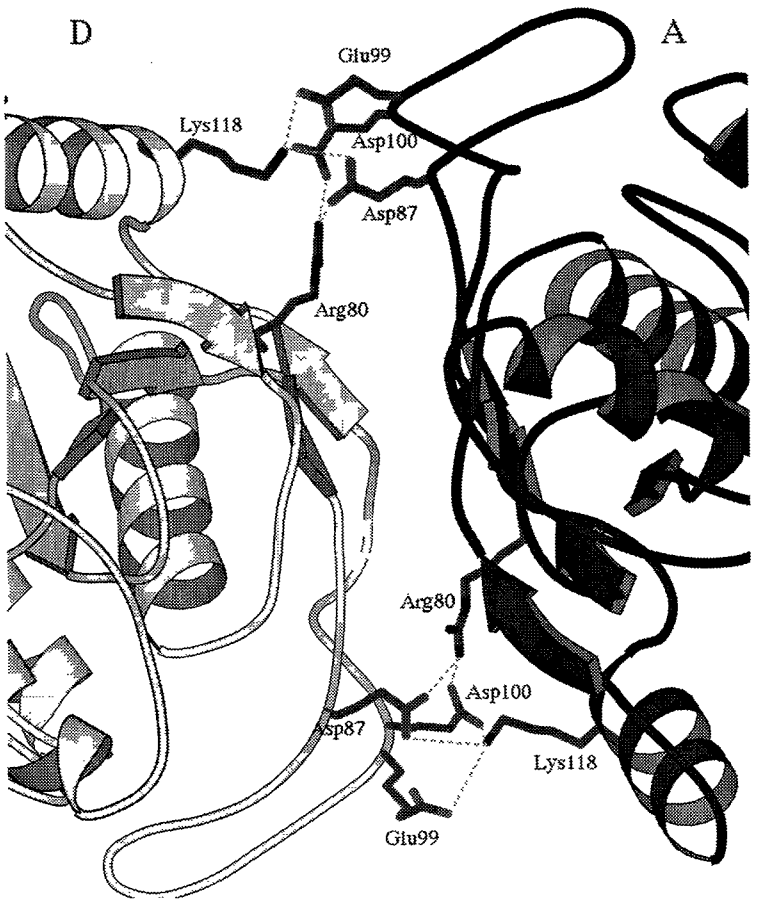
D
A
Glu99
Lys118
Asp100
Asp87
Arg80
Arg80
Asp100
Asp87
Lys118
Glu99

b) *Ba*PCP

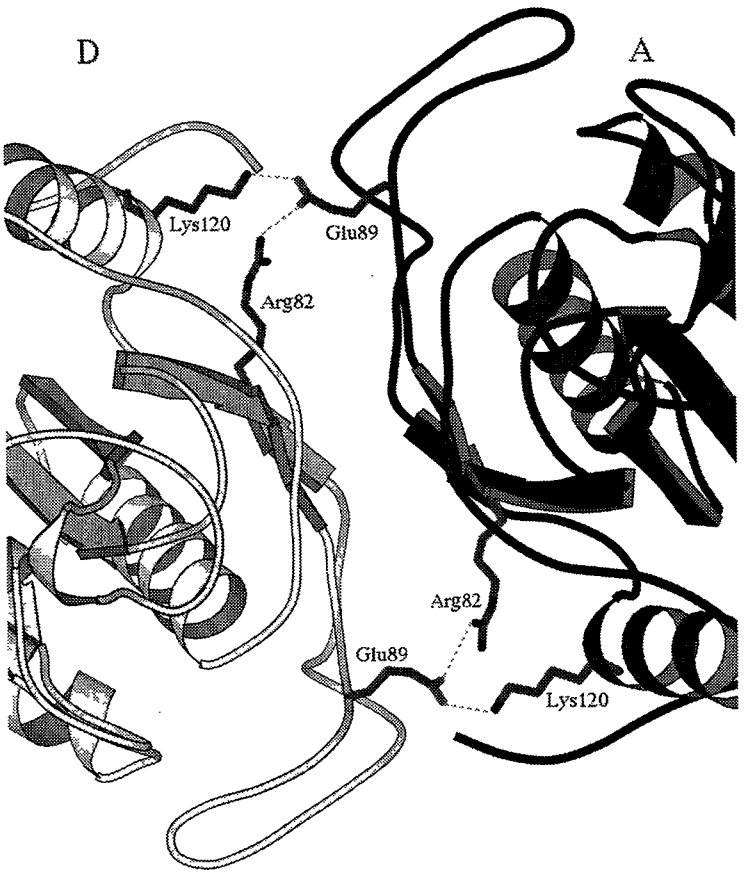

c) *TlPCP*

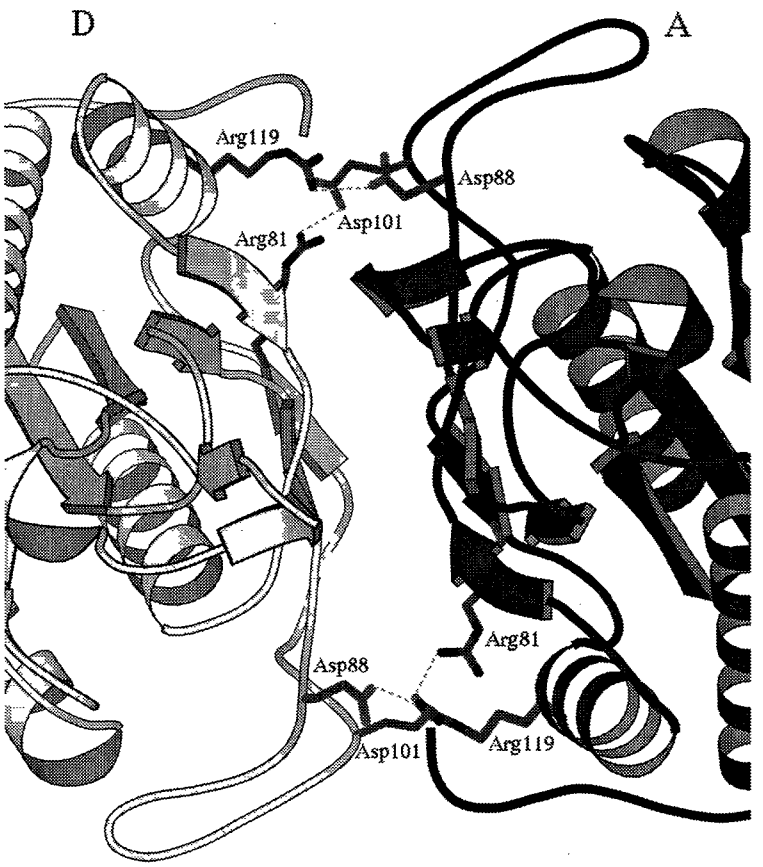

Figure 2-8. Comparison of ion pairs between subunits A and D for the three proteins, *Pf*PCP (a), *BaPCP* (b), *TlPCP* (c). There are ten salt bridges at each interface in *Pf*PCP, Asp80-Arg87, Asp87-Lys118, Glu99-Lys118, Asp100-Arg80, and Asp100-Lys118, and its noncrystallographic symmetry-related pairs form salt bridge interactions. The figure was produced using MOLSCRIPT (Kraulis, P. J., 1991).

the mesophile PCP. The ion pairs of three PCPs within 4 Å are listed in Table 2-3. Figure 2-8 shows the ion pairs between subunit A and D for three proteins. There were ten ion pairs at each interface in the case of *Pf*PCP. That of *T1PCP* and *Ba*PCP was 6 and 4, respectively.

In *Pf*PCP, a polar amino acid, Glu192, was found in the interior of the molecule (Figure 2-9). The environment of Glu192 was completely surrounded by hydrophobic residues, Pro18, Ile22, Ile76, Val167, Pro168, Ile170, Met187, Ala195 and Val196. Negatively charged residues are usually located in the N-terminal of an a helix as a helix cap, but Glu192 was in the C-terminal of the a helix (α6), suggesting the destabilization effect. But a distance between carboxyl oxygen atom of Glu192 and oxygen atom of Pro168 was 2.95 Å, which suggested that the protonated carboxyl group of Glu192 had a hydrogen bond with the carboxyl oxygen of Pro168. This buried polar residue is conserved in *T1PCP* (Glu194) in the hydrophobic surrounding, and its three-dimensional arrangement is also similar to that in *Pf*PCP. On the other hand, the corresponding residue of *Ba*PCP is Ile189 and is also in the hydrophobic interior.

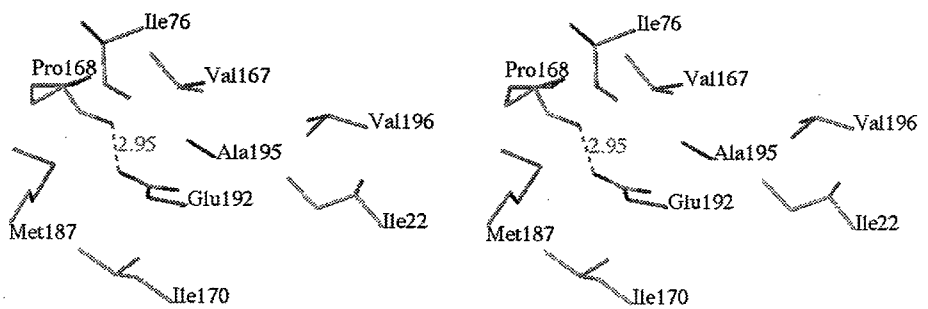

Figure 2-9. The structure surrounding glutamic acid 192 of the *Pf*PCP in the hydrophobic interior of a molecule. The distance between the carboxyl oxygen atom of Glu192 and the oxygen atom of Pro168 was 2.95 Å.

Chapter 3

The thermal stability of *Pf*PCP

3-1 Introduction

The thermal stability of *Pf*PCP is considerably high compared with that of *Ba*PCP: the peak temperature of the DSC curves is 104.5 and 62.9 °C for *Pf*PCP and the *Ba*PCP, respectively, at pH 9.5 (Ogasahara et al., 2001). If Cys-188 in *Pf*PCP forms a disulfide bond between subunits, the stability further increases: the peak temperature of the DSC curves is 116.5 °C at pH 9.5. On the other hand, *Tl*PCP seems to be less stable than *Pf*PCP (a half-life of two hours at 75 °C (Singelton et al., 2000)), although it comes from a hyperthermophile archaeon. The stabilization mechanism of *Pf*PCP was investigated on the basis of structural differences among the three proteins, *Pf*PCP, *Tl*PCP, and *Ba*PCP.

3-2 Contribution of the Hydrophobic Interaction

The hydrophobic interaction in the interior of a protein is one of the important stabilizing forces (Kauzman, 1959). Takano et al. (1998) have found a general rule for the relationship between a hydrophobic effect

and the conformational stability of a protein, using a series of hydrophobic mutants of human lysozyme. The change in unfolding Gibbs energy (ΔG) due to a hydrophobic effect between wild-type and mutant proteins ($\Delta\Delta G_{HP}$) can be expressed using changes in accessible surface area (ASA) of non-polar and polar atoms due to denaturation as follows (Funahashi et al., 1999):

$$\Delta\Delta G_{HP} = \alpha\Delta\Delta ASA_{non\text{-}polar} + \beta\Delta\Delta ASA_{polar} \quad (1)$$

where $\Delta\Delta ASA_{non\text{-}polar}$ and $\Delta\Delta ASA_{polar}$ represent the differences in ΔASA of non-polar and polar atoms of all residues in a protein, respectively, upon denaturation between wild-type and mutant proteins. Using the stability/structure database for a series of mutant human lysozymes, the parameters α and β have been determined to be 0.178 and -0.013 kJ mol^{-1} $Å^{-2}$, respectively (Funahashi et al., 1999). ASA values of proteins in the native state can be calculated using X-ray crystal structures, and those in the denatured state using their extended structures. For the calculation of ASA, C/S atoms in residues were assigned to $ASA_{non\text{-}polar}$ and N/O to ASA_{polar}.

We tried to estimate the contribution of the hydrophobic interaction of *Pf*PCP, *Tl*PCP, and *Ba*PCP tor the stabilization ($\Delta\Delta G_{HP}$). ASA values using X-ray crystal

structures of the three proteins in the native state were calculated using the procedure of Connolly (1993). The ASA values in the denatured states were calculated from their extended structures of each protein, which were generated from the native structures using Insight II. As shown in Table 3-1, the $_{\Delta}G$ values due to hydrophobic interaction (ΔG_{HP}) of *Pf*PCP was greater than that of *Ba*PCP: the $\Delta\Delta G_{HP}$ values between *Pf*PCP and *Ba*PCP were 63 and 43 kJ/mole of a monomer, assuming a monomer in the native state and a tetramer in the native state, respectively. However, those of *Pf*PCP were smaller than those of *Tl*PCP. These results indicate that the higher stabilities of *Pf*PCP and *Tl*PCP are caused by the hydrophobic interaction. The content of hydrophobic residues (total residues of Ile, Val, Leu, Phe, Cys, Met, and Ala) was 41.9, 40.0, 37.7 % for *Pf*PCP, *Tl*PCP, and *Ba*PCP, respectively. Although the content of *Tl*PCP is not highest, the higher hydrophobic effect of *Tl*PCP might come from buried hydrophobic ethylene groups of Lys and Arg, which contribute to hydrophobic interaction.

3-3 Stability Analysis of the PCP Structures by Knowledge-Based Potential

Ota et al., (1995) have proposed that the

Table 3-1. The contribution of hydrophobic interaction to conformational stability of three PCPs

protein	ΔASA(C/S)	ΔASA(N/O)	ΔG_{HP}	$\Delta\Delta G_{HP}$
*Ba*PCP	13530	5997	2330	
4*Ba*PCP*	58545	25838	2521	
*Tl*PCP	14874	5950	2570	240
4*Tl*PCP*	65800	26794	2841	320
*Pf*PCP	13860	5672	2393	63
4*Pf*PCP*	59430	24728	2564	43

The unit of ΔASA and ΔG is $Å^2$ and kJ/mol of monomer, respectively. $\Delta\Delta G_{HP}$ represents the difference in ΔG_{HP} between mesophile and hyperthermophile proteins. *Tetramer PCP

changes in conformational stability due to a single amino acid substitution can be calculated by SPMP (Stability Profiles of Mutant Proteins), using their X-ray structures. In SPMP, a pseudo-energy potential ($\Delta\Delta G_{SPMP}$) developed for evaluating structure-sequence compatibility in the structure prediction method is employed, consisting of four elements: side-chain packing ($\Delta\Delta G_{SP}$), hydration ($\Delta\Delta G_{Hyd}$), local structure ($\Delta\Delta G_{LC}$) and back-bone-side-chain repulsion ($\Delta\Delta G_{BR}$) (Ota et al., 1995; Takano et al., 1999).

$$\Delta\Delta G_{SPMP} = \Delta\Delta G_{SP} + \Delta\Delta G_{Hyd} + \Delta\Delta G_{LC} + \Delta\Delta G_{BR} \qquad (2)$$

The pseudo-energy potential provides a fitness score for each residue type of a site in a native structure. The estimation of $\Delta\Delta G$ for a replacement of residue X by residue Y is as follows.

$$\Delta G(X) = \langle G(X) \rangle - G(X)$$
$$= G^D(X) - G^N(X) \qquad (3)$$
$$\Delta\Delta G(X \rightarrow Y) = \Delta G(Y) - \Delta G(X)$$
$$= [G^D(Y) - G^N(Y)] - [G^D(X) - G^N(X)]$$
$$= [G^D(Y) - G^D(X)] - [G^N(Y) - G^N(X)] \qquad (4)$$

where $G(X)$ and $\langle G(X) \rangle$ represent the fitness score for residue X of a site in a native structure calculated by the potential and the reference score, respectively, corresponding to the Gibbs energy in the native and

denatured states for residues X, $G^N(X)$ and $G^D(X)$, respectively.

The conformational stabilities of the three PCP structures were analyzed using SPMP. The individual stability score of four terms are summarized in Table 3-2. The difference in the total score of the PCPs from hyperthermophiles and mesophile, e.g., *Tl* – *Ba* and *Pf* – *Ba*, explains the significant stability of both hyperthermophile PCPs very well; however, the contributions of each score term were slightly different. *Tl*PCP appears to be stabilized mainly by the side-chain packing term, while the hydration and local structural terms are the contributors to *Pf*PCP stabilization. Although it is not easy to interpret the side-chain packing and hydration terms individually because both of them originate from the hydrophobic interaction, it seems that the packing pattern of *Pf*PCP is simpler than that of *Tl*PCP: hydrophobic and hydrophilic residues are located on the interior or exterior of the protein structure, respectively, and *Tl*PCP has a more preferable side-chain arrangement than the *Pf*PCP. In a tetramer conformation, the stability score of *Pf*PCP was the highest.

Fitness of PCP sequence at each position was estimated by the knowledge-based function (SPMP). Comparing the stability score of each residue for *Pf*PCP

Table 3-2. SPMP stability scores of each PCP structure

a) monomer

structure	Total	SP	Hyd	LC	BR
*Ba*PCP	400.8	302.0	50.6	106.6	-58.1
*Tl*PCP	419.2	314.2	46.8	122.5	-64.4
*Pf*PCP	455.2	306.6	70.2	136.3	-58.1
Tl - Ba	18.4	12.1	-3.7	15.4	-6.2
Pf - Ba	54.3	5.0	19.6	29.2	0

b) tetramer

structure	Total	SP	Hyd	LC	BR
4 *Ba*PCP	423.4	320.0	58.1	106.6	-61.9
4 *Tl*PCP	468.1	353.5	60.6	122.5	-68.6
4*Pf*PCP	490.3	321.3	93.3	136.3	-61.0
4*Tl - 4Ba*	44.7	33.4	2.5	15.8	-6.6
4*Pf - 4Ba*	66.9	1.2	35.1	29.7	0.8

The unit is kJ/mol. Positive values show the stabilization. *Pf–Ba* and *Tl-Ba* represent the difference of total scores between *Pf*PCP and *Ba*PCP, and between *Tl*PCP and *Ba*PCP, respectively. SP, Hyd, LC, and BR means contribution due to side-chain packing ($\Delta\Delta G_{SP}$), hydration($\Delta\Delta G_{Hyd}$), local structure ($\Delta\Delta G_{LC}$) and back-bone-side-chain repulsion ($\Delta\Delta G_{BR}$) , respectively, in each residue (eq. 2).

with that of the corresponding residue for *Ba*PCP, we can investigate the important residues of *Pf*PCP for its conformational stability. The top 10 in differences are listed in Table 3-3, suggesting which residues of *Pf*PCP contributes to the stability as compared with the *Ba*PCP.

The largest difference in the stability scores is between Ile31 of *Pf*PCP and Glu33 of *Ba*PCP. Ile31 is involved in a β strand and Ile exhibits strong β intensity. Also it interacts with Ile29, Val36, Ile200, and Ile204, and they constitute a small hydrophobic cluster near the protein surface. Whereas, Glu33 of *Ba*PCP interacts only with Lys194 and they form a salt-bridge. Tyr169 of *Pf*PCP (Tyr171 of *Ba*PCP) gains the score by the interactions with Gln14, Pro71 and Lys177. On the other hand, Tyr171 and Gly73 appear too close in the *Ba*PCP structure. Pro105 of *Pf*PCP (Gln107 of *Ba*PCP) is strongly suitable for the local structure around this site: extended coil (position 104) - extended coil (position 105) - left-handed helix (position 106). Tyr132 of *Pf*PCP (Ala134 of *Ba*PCP) of the A chain interacts with Ala75 and Ser77 of the chain and Val183 of the C chain. Moreover, Tyr shows more preferable β propensity than Ala. Ile78 of *Pf*PCP (Pro80 of *Ba*PCP) is in hydrophobic environments: Ile171, Ile120, Met121, Leu124, Ile113 and Ile165. Around Pro80 in *Ba*PCP, there are also Ile119, Ile122 and Ile167, yet the interactions

Table 3-3. The top ten residues in the difference of SPMP scores between *Pf*PCP and *Ba*PCP

No.	*Pf–Ba*	Protein	Site	Total	SP	Hyd	LC	BR
1	9.83	*Pf*PCP	31Ile	5.36	2.89	0.96	1.63	-0.13
		*Ba*PCP	33Glu	-4.48	-1.76	-1.21	-1.38	-0.13
2	7.45	*Pf*PCP	169Tyr	2.47	5.48	0.59	-0.63	-3.01
		*Ba*PCP	171Tyr	-4.98	-1.84	-0.13	-0.79	-2.18
3	6.40	*Pf*PCP	105Pro	6.23	0.46	1.42	4.39	0
		*Ba*PCP	107Gln	-0.17	0.17	0.54	-0.88	-0.04
4	6.07	*Pf*PCP	132Tyr	5.10	2.43	1.05	1.80	-0.21
		*Ba*PCP	134Ala	-0.96	-0.29	-0.25	-0.46	0
5	5.94	*Pf*PCP	78Ile	7.03	4.27	1.51	1.63	-0.42
		*Ba*PCP	80Pro	1.09	2.72	-0.96	-0.63	-0.08
6	5.56	*Pf*PCP	205Glu	2.05	-0.18	1.21	1.09	-0.08
		*Ba*PCP	202Val	-3.51	0.08	-1.21	-2.13	-0.25
7	5.48	*Pf*PCP	193Leu	2.22	2.93	-1.55	1.09	-0.25
		*Ba*PCP	190Thr	-3.26	-0.75	0.29	-2.64	-0.17
8	5.31	*Pf*PCP	124Leu	10.42	8.58	1.72	0.63	-0.50
		*Ba*PCP	126Ile	5.10	3.26	1.88	0.67	-0.67
9	5.02	*Pf*PCP	152His	2.18	2.05	-0.54	0.79	-0.13
		*Ba*PCP	154Glu	-2.85	-0.75	-2.05	0.84	-0.84
10	4.77	*Pf*PCP	151His	4.43	3.43	0.29	0.79	-0.08
		*Ba*PCP	153Asp	-0.33	3.47	-1.84	-1.80	-0.13

Pf–Ba represents the difference of total scores between *Pf*PCP and *Ba*PCP. SP, Hyd, LC, and BR means contribution due to side-chain packing ($\Delta\Delta G_{SP}$), hydration ($\Delta\Delta G_{Hyd}$), local structure ($\Delta\Delta G_{LC}$) and back-bone-side-chain repulsion ($\Delta\Delta G_{BR}$), respectively,

in each residue (eq. 2). The unit of score is kJ/mol. are less than in the former case. Glu205 of *Pf*PCP (Val202 of *Ba*PCP) on the helix C-terminal and partially buried site is more suitable than Val. Leu124 of *Pf*PCP (I126 of *Ba*PCP): Leu124 of *Pf*PCP interacts with more hydrophobic residues (Ile76, Ile78, Ile120, Ile129, Ala131, Ala195 and Val198) than the equivalent residue of *Ba*PCP, Ile126, interacting with Ile78, Ile131, Ala133 and Ile195.

SPMP provides stability scores for each residue at every site. In the case of *Pf*PCP (208 amino acid residues), the stability changes upon mutation, $\Delta\Delta G$, of 208x19 mutants were predicted by SPMP (Ota et al., 1995) using the crystal structure of *Pf*PCP. 30.3 % of the native residues of *Pf*PCP ranked at the top of 20 kinds of residues: that of *Ba*PCP was 27.9 %. The average ranking of all native residues among 20 amino acids for *Pf*PCP and *Ba*PCP was 4.95 and 5.74, respectively. These results indicate that the sequence of the hyperthermophile protein (*Pf*PCP) is more fitted to an ideal structure than that of the mesophile protein (*Ba*PCP).

3-4 Contribution of Ion Pairs (Salt Bridges)

In hyperthermophile proteins, it has been reported that ion pair networks on the protein surface are usually

assumed to be stabilizing (Yip and Consalvi, 1995; Hennig et al, 1995; Pappenberger et al, 1997). Table 3 lists the ion pairs formed within 4 Å for the three PCPs. The number (0.10) of ion pairs per residue for the *Pf*PCP is similar to that (0.09) for *Ba*PCP but greater than that (0.07) for *Tl*PCP. They were greater than that (0.04) of the average number of mesophile proteins (Barlow, 1983). In *Pf*PCP, 31 residues are involved in the formation of 20 ion pairs: 6 ion pairs with 6 residues form an ion pair network between subunits (A and D, or B and C) (Figure. 2-8-a). In *Ba*PCP, 5 ion pairs with 6 residues form an intramoleculer ion network. *Tl*PCP has only a small ion network between subunits (4 ion pairs with 5 residues). An intramoleculer ion-network in a mesophilic protein (*Ba*PCP), which is almost buried in the interior of the molecule, disappears in hyperthermophile proteins (*Pf*PCP and *Tl*PCP). Ion pairs between subunit A and D were partly conserved in the three proteins, but those of *Pf*PCP form an intersubunit network and seem to contribute to its higher stability of the tetramer (Figure 2-8).

3-5 Contribution of Hydrogen Bonds

Hydrogen bonds are ubiquitous in proteins, and their contribution to the conformational stability is of

fundamental importance, as is the hydrophobic interaction. Recently, the net contribution of an intramolecular hydrogen bond has been estimated to be 8.5 kJ/mol for a 3 Å-long hydrogen bond using a series of hydrogen bond mutants of human lysozyme (Takano et al., 1999). The average number of hydrogen bonds per residue for *Pf*PCP, *Tl*PCP, and *Ba*PCP is 2.086, 2.064, and 1.986, respectively. The total number of hydrogen bonds for the *Pf*PCP (434/208 residues) was greater than that of the *Ba*PCP (417/210 residues) but comparable to that of *Tl*PCP (454/220 residues). The increase in 17 hydrogen bonds corresponds to stabilization by 144 kJ/mol. These results suggest that the hydrogen bonds of both hyperthermophile proteins considerably contribute to higher thermostabilities compared with the mesophile protein. In addition to intrasubunit hydrogen bonds, there were 10, 14, and 2 intersubunit hydrogen bonds for the *Pf*PCP, *Tl*PCP, and *Ba*PCP, respectively. This indicates that both hyperthermophile proteins are also more stabilized by the subunit interaction of hydrogen bonds than the mesophile protein.

3-6 Other Contributions to Stability

One of the important stabilizing factors is an

entropic effect when the conformational entropy of a protein is decreased in the denatured state due to substitutions or deletion. They correspond to the introduction of disulfide bonds, substitution of other residues with Pro, and shortening of polypeptides. The X-ray structure of *Pf*PCP indicates that Cys188 in *Pf*PCP does not form a disulfide bond, although the corresponding Cys190 in *Tl*PCP does (Singleton et al., 1999). *Pf*PCP is expressed in an *E. coli* strain that cloned only the PCP gene from *P. furiosus*. The Cys188 is partly oxidized during the purification process, and its oxidized *Pf*PCP is considerably stable as compared with the counterpart (Ogasahara et al., submitted). The X-ray structure of *Pf*PCP also indicates that Cys188 is capable of a disulfide bond between subunits. Therefore, the *Pf*PCP expressed under the physiological conditions of *P. furiosus* around 100 °C might form an intersubunit disulfide bond at Cys188 to stabilize the conformation.

The contents of the Pro residue were 15 to 16 for the three proteins, suggesting that there is no difference in stability due to the Pro contents. The total residues for *Pf*PCP, *Tl*PCP, and *Ba*PCP were 208, 220, and 215, respectively. We can calculate the entropic effects of denaturation from their amino acid compositions using thermodynamic parameters proposed by Oobatake and Ooi

(1993): the denaturation entropy for the *Pf*PCP, *Tl*PCP, and *Ba*PCP is 0.67, 0.67, and 0.40, kJ mol^{-1} K^{-1}, respectively. This indicates that both hyperthermophile proteins are not stabilized by their entropic effect.

The increase in cavity volume in the interior of a protein decreases the conformational stability. The contribution (ΔG) of the changes in the cavity volume to the protein stability has been estimated to be – 0.100 and –0.073 kJ mol^{-1} $Å^{-3}$, using some mutant T4 lysozymes (Eriksson et al., 1992) and data for both mutant human and T4 lysozymes (Funahashi et al., 2001), respectively. For the tetramers of the three PCPs, the cavity volume was determined by attempting to insert a probe sphere of 1.4 Å radius (assuming a water molecule) (Connolly, 1993). The total volume of the cavity for *Pf*PCP, *Tl*PCP, and *Ba*PCP was 973, 622, and 1129 $Å^3$, respectively. This result indicates that *Tl*PCP is considerably more stabilized due to the decrease in cavity volume, but *Pf*PCP is comparable to *Ba*PCP.

Ionized amino acids in globular proteins are almost exclusively on the outside exposed to the solvent, while those in the interior of a protein are believed to form ion pairs or play essential roles in function and stability. Glu192 in *Pf*PCP is 100 % buried in the hydrophobic core, and the corresponding Glu194 in *Tl*PCP is also completely

buried, suggesting that the buried Glu residue is conserved in hyperthermophiles. On the other hand, the corresponding residue of a mesophile protein, *Ba*PCP, is replaced by a hydrophobic residue, Ile195, that might play an important role in hydrophobic interaction. Both Glu residues of hyperthermophiles, which do not have any ion pairs, seem to contribute to destabilizing. If the Glu residues are substituted by hydrophobic residues, the mutant protein should be stabilized. However, all hydrophobic mutant *Pf*PCPs at Glu 192 were less stable than the wild-type protein (in this case Cys-free *Pf*PCP was used) (in preparation). The OE1 atom of Glu192 in *Pf*PCP is close to the O atom of Pro168 (2.95 Å): the OE2 atom of Glu 194 in the *Tl*PCP is also close to the O atom of Pro169 (2.62 Å). This suggests that if the Glu192 (Glu194) is protonated, the protonated Glu might forms a hydrogen bond with the O atom of Pro. However, at present, it is difficult to explain how the conserved buried Glu residues in hyperthermophiles play an important role in stabilization.

Chapter 4

Crystals of novel virus from *Pyrococcus furiosus*

4-1 Introduction

I have tried to crystallize the 80S ribosome from yeast (*Saccharomyces carlsbergensis*) since 1995. The number of tested conditions for crystallization reached thousands or more. But yeast 80S ribosome was unstable in the conditions for crystallization, and I could not get crystal of this assembly. Therefore, I decided to change the species from yeast to thermophilic bacteria whose proteins are very stable even at high temperature. The hyperthermophile, *Pyrococcus furiosus*, belongs to archae and they can grow at high temperatures (88 ~ 104 °C), favoring a temperature of 98°C. I have selected this bacteria for the starting material, and tried to crystallize the ribosome.

The purification procedure of 70S ribosome from *P. furiosus* with high purity and high activity was established. No column chromatography was applied for the purification to avoid removal of ribosomal components. The 70S ribosome was successfully purified with high activity by the centrifugation, ultra-centrifugation and density gradient centrifugation (Figure 4-2, 4-3, 4-4 4-5

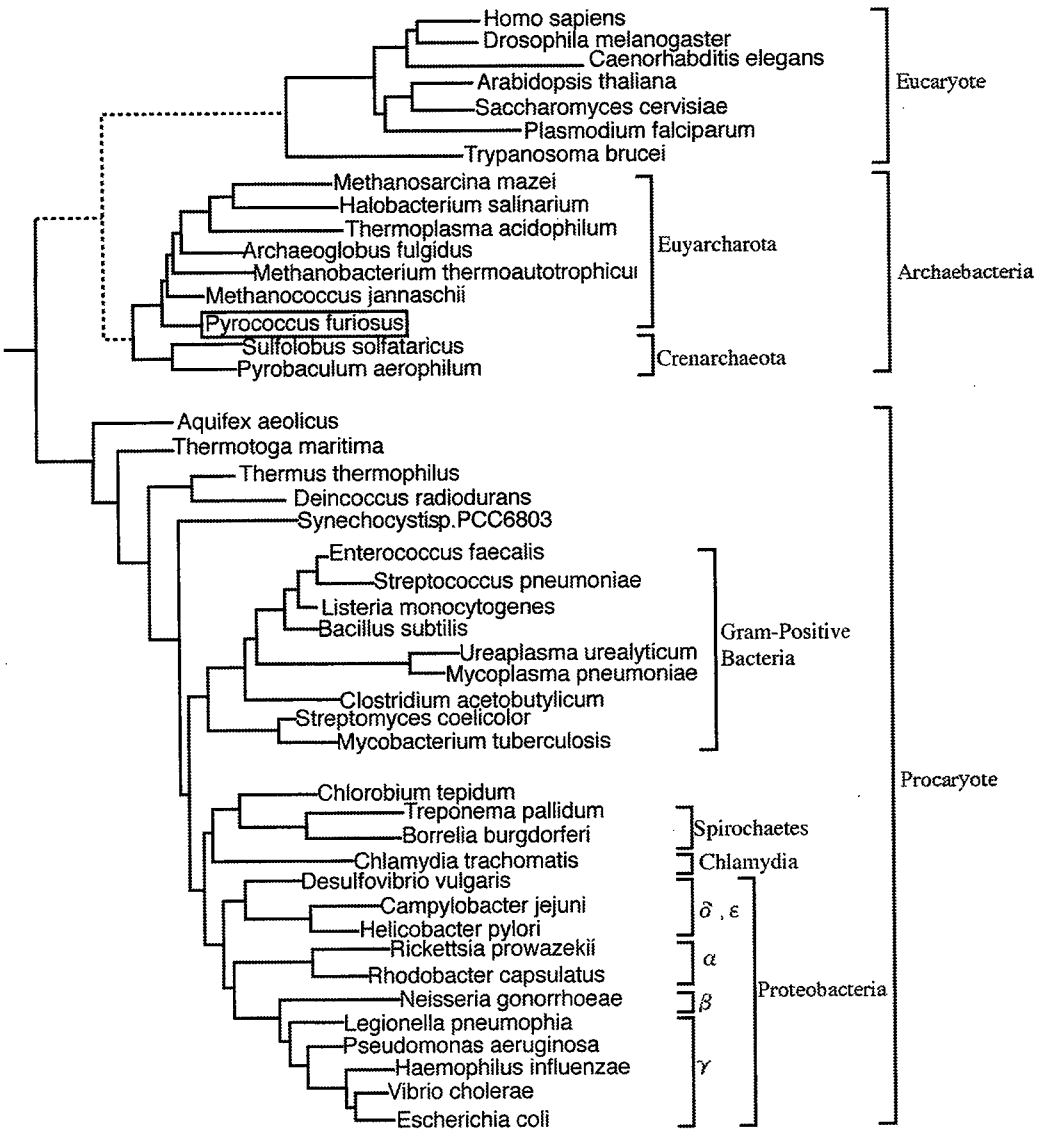

Figure 4-1. Phylogenetic tree based on small-subunit rRNA coding sequences. Each phylogenetic tree was proposed separately and they were connected.

and Table 4-1), and some crystals were obtained from several conditions. Unfortunately component of these crystals were not ribosome, but a spherical particle with larger molecular weight than the 70S ribosome. Further research showed that component of these crystals was for a novel virus and its gene was integrated in the *P. furiosus* gene.

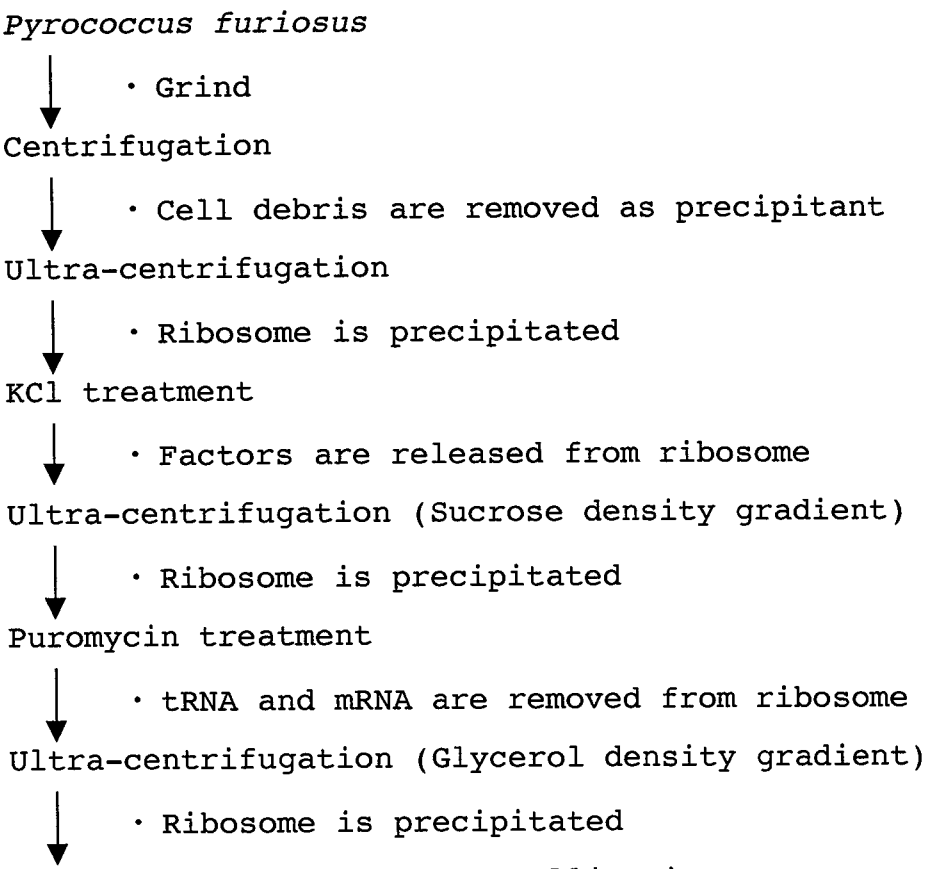

Figure 4-2. A scheme of purification procedure of 70 S ribosome.

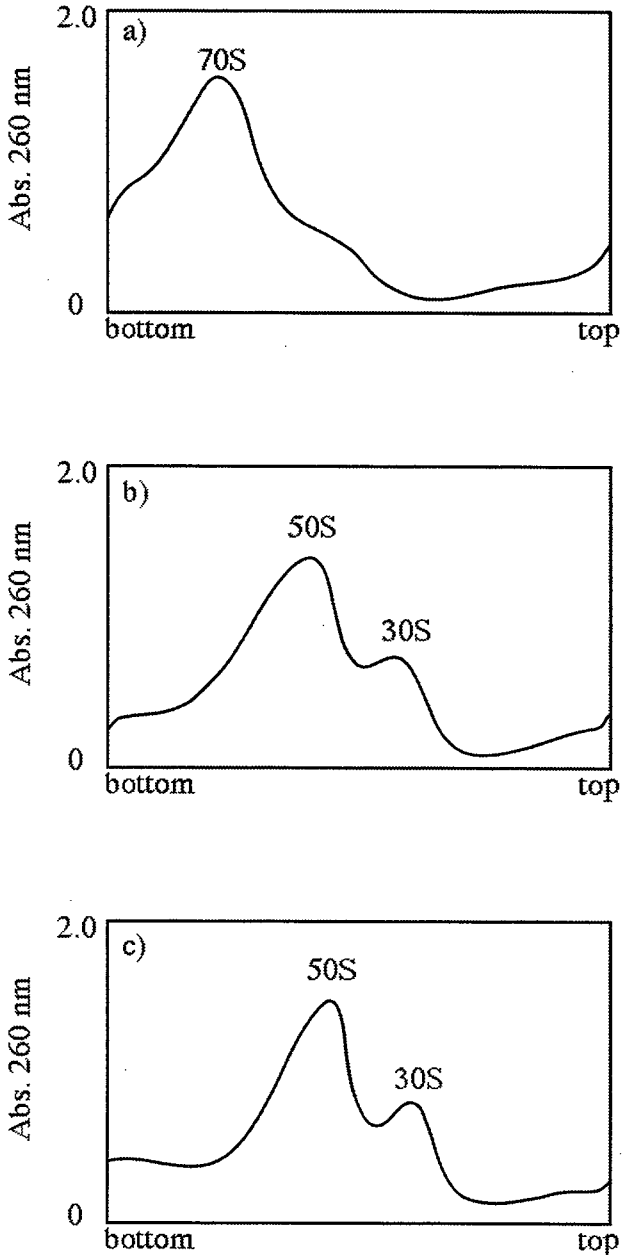

Figure 4-3. Resuluts of sucrose gradient analysis of 70S ribosome. a) 30 mM $MgCl_2$, b) 3 mM $MgCl_2$, c) 3 mM $MgCl_2$ and 500 mM KCl

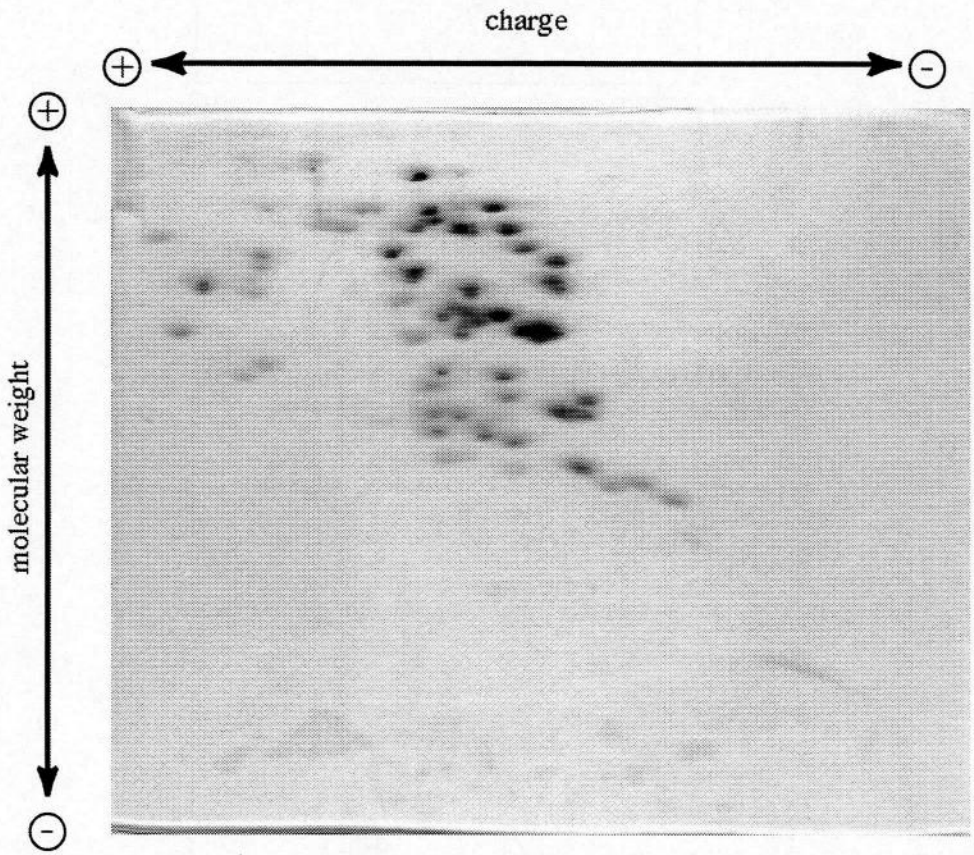

Figure 4-4. Electrophoregrams of ribosomal proteins prepared from *Pyrococcus furiosus* 70S ribosome. A total of 65 spots were identified in this experiments.

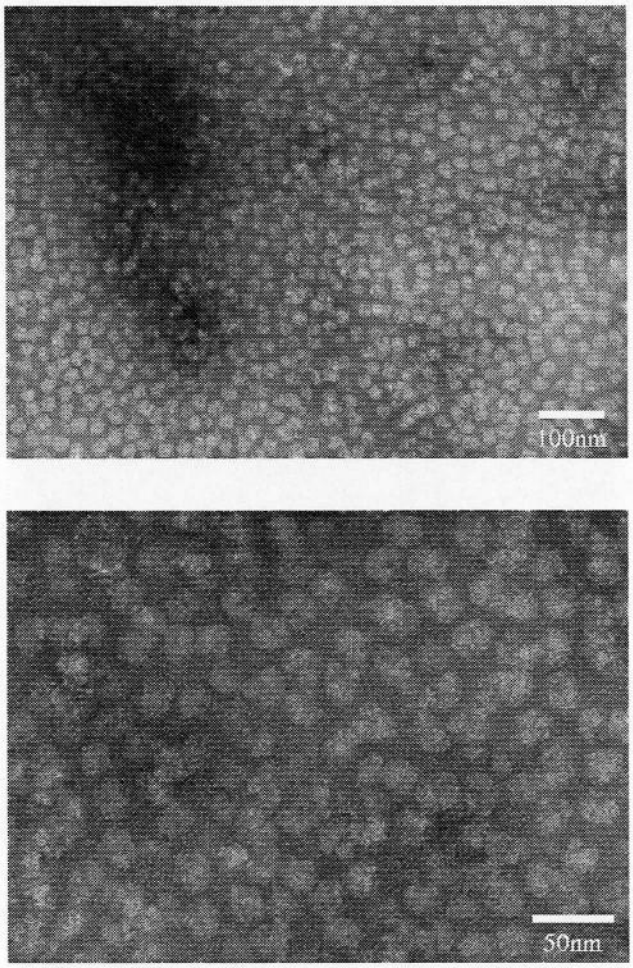

Figure 4-5. Electron micrograph of negatively stained 70S ribosome from *Pyrococcus furiosus*. Each particle is about 25 ~ 27 nm in diameter and composed of two subunits, large and small.

Table 4-1. Results of activity measurement of 70S ribosome from *Pyrococcus furiosus*.

Conditions	Radio activity [cpm]
1) poly(U) + tRNA + S-100	11.3
2) poly(U) + tRNA + ribosome	43.7
3) tRNA + ribosome + S-100	148.7
4) poly(U) + tRNA + ribosome + S-100	1634.0
5) poly(U) + ribosome + S-100	2235.5

4-2 Survey of crystallization conditions

4-2-1 Methods for attaining supersaturation

The protein solution must be supersaturated prior to nucleation of crystal. There are mainly three methods for attaining supersaturation, vapor diffusion method, dialysis method and batch method. Hanging drop vapor diffusion method was used to examine conditions for the crystallization of virus. A 5 μl drop of protein solution placed on a cover glass (18 mm x 18 mm, IWAKI glass, Japan) was mixed with the same volume of reservoir solution (precipitant). The wells containing precipitant solution were covered with cover glasses hanging the drop, and they were incubated at various temperature (Figure 4-6). The 24 well disposable plastic tissue culture plates (model 3820-024N, IWAKI glass, JAPAN) were used for this experiment.

The hanging drop vapor diffusion method always gave bigger crystals. Other crystallization methods such as micro-batch method, micro-dialysis method, sitting drop and sandwich drop vapor diffusion methods did not produce any good crystals. The micro-dialysis method gave no crystals. The micro-batch method gave very small crystals

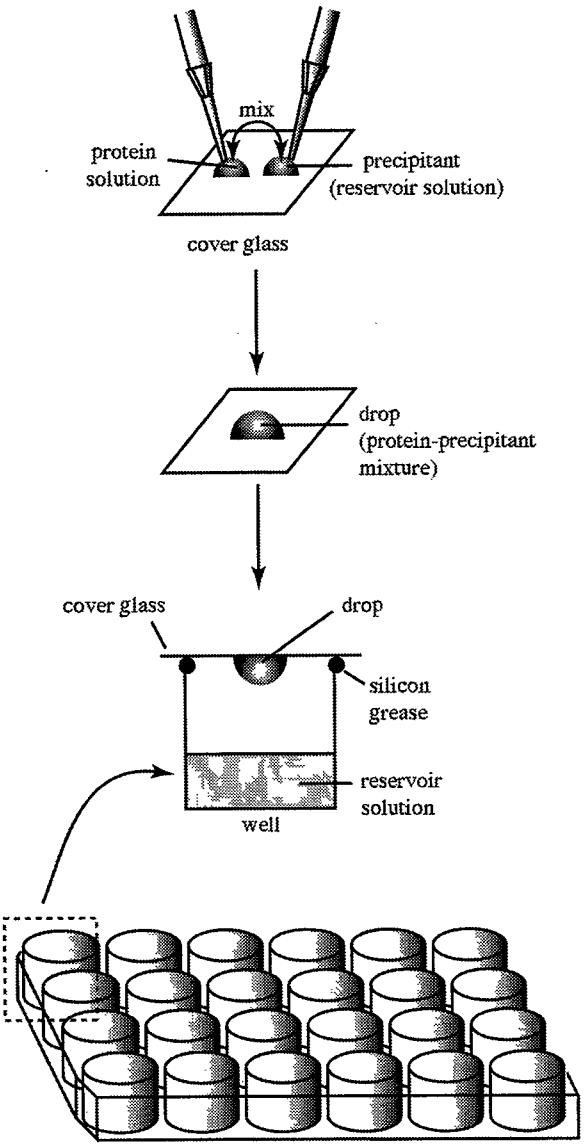

Figure 4-6. Hanging drop vapor diffusion method

The protein solution placed on cover glass was mixed with the same volume of reservoir solution. The wells containing precipitant solution were covered with them.

occasionally. The sitting drop and sandwich drop vapor diffusion methods gave only small crystals. The condition of hanging drop vapor diffusion method was optimized for the present crystallization.

4-2-2 Protein concentration

Protein concentration is one of the important factors for crystallization. They affect degree of supersaturation of protein solution. In this crystallization study, protein concentrations were varied from 20 mg/ml to 100 mg/ml in 10 mg/ml steps. Crystals grew at all these protein concentrations.

4-2-3 Temperature

Temperature which affected the solubility of 70S ribosome was very important factor. Crystallization was carried out at four different temperatures of 4, 15, 20 and 25 °C. There were no crystals at 4 °C. Crystal was grown at 15 and 20 °C.

4-2-4 pH and Buffer

Since the pH of the solution affects the solubility

of the protein, varying pH of the solution is one of the effective strategy for crystallization. But each enzyme has an individual optimum pH, and its activity is high in the limited range of pH. Therefore, screening must be carried out near the optimum pH (pH 7.5) for the ribosome. The pH was varied between pH 6.0 and pH 10.0 in the survey of conditions for crystallization. The buffers used for crystallization trials of 70S ribosome were showed in Table 4-2.

4-2-5 Precipitant

Although there is a lot of precipitating reagents for macromolecular crystallization, they are roughly divided into three categories: salts such as ammonium sulfate and sodium chloride; organic solvents such as ethanol and MPD; and polymers such as polyethylene glycol (PEG). Ammonium sulfate, sodium chloride, potassium chloride, ethanol, MPD, PEG-1000, PEG-4000, PEG-6000, PEG-8000, PEG-10000 and PEG-20000 were tested as precipitating reagents for 70S ribosome.

4-3 Results

Different three kinds of crystals were grown under

Table 4-2. Buffers used for crystallization

pH range	Buffer
6.0 –7.0	MES, Cacodylate
7.0 –8.0	Hepes, Tris
8.0 –9.0	Tris
9.0 –10.0	Glycine

the different crystallization conditions in this experiment. All the conditions for crystallization were shown in Table 4-3. The best protein concentration range to grow large crystals was 40 ~ 60 mg/ml. The largest crystals were obtained at 25 °C. Thus the incubation temperature was fixed at 25 °C. Tetragonal bi-pyramidal crystals were obtained from 20 ~ 25 % (v/v) MPD (Figure 4-7). These crystals grew up to 0.05 mm x 0.05 mm x 0.01 mm at 25 °C in 1 week. Another tetragonal bi-pyramidal crystals were also obtained from 20 %(w/v) PEG 1000 (Figure 4-8). These crystals grew to 0.02 mm x 0.02 mm x 0.005 mm at 25 °C in 1 week. This crystal was similar to MPD crystal in morphology. Diamond shape crystals were also obtained from 4 ~ 8 %(w/v) PEG 4000 (Figure 4-9). These crystals grew to 0.02 mm x 0.02 mm x 0.005 mm at 25 °C in 2 days.

4-4 Optimization of crystallization condition

4-4-1 Introduction

The crystals obtained from MPD, PEG-1000 and PEG-4000 were very small, and unsuitable for X-ray irradiation. Nucleation and growth rate of the crystal should be reduced to get bigger crystals. The various

Table 4-3. Crystallization conditions

a) Crystals from MPD

Method	Hanging drop
Buffer	20 mM Tris-HCl
pH	7.5
Protein concentration	40 ~ 60 mg/ml
Precipitant	MPD
drop	12.5 % (v/v)
reservoir	25 % (v/v)
Temperature	25 °C

b) Crystals from PEG-1000

Method	Hanging drop
Buffer	20 mM Tris-HCl
pH	7.5
Protein concentration	40 ~ 60 mg/ml
Precipitant	PEG-1000
drop	12.5 % (v/v)
reservoir	25 % (v/v)
Temperature	25 °C

c) Crystals from PEG-4000

Method	Hanging drop
Buffer	20 mM Tris-HCl
pH	7.5
Protein concentration	40 ~ 60 mg/ml
Precipitant	PEG-4000
drop	8 % (v/v)
reservoir	16 % (v/v)
Temperature	25 °C

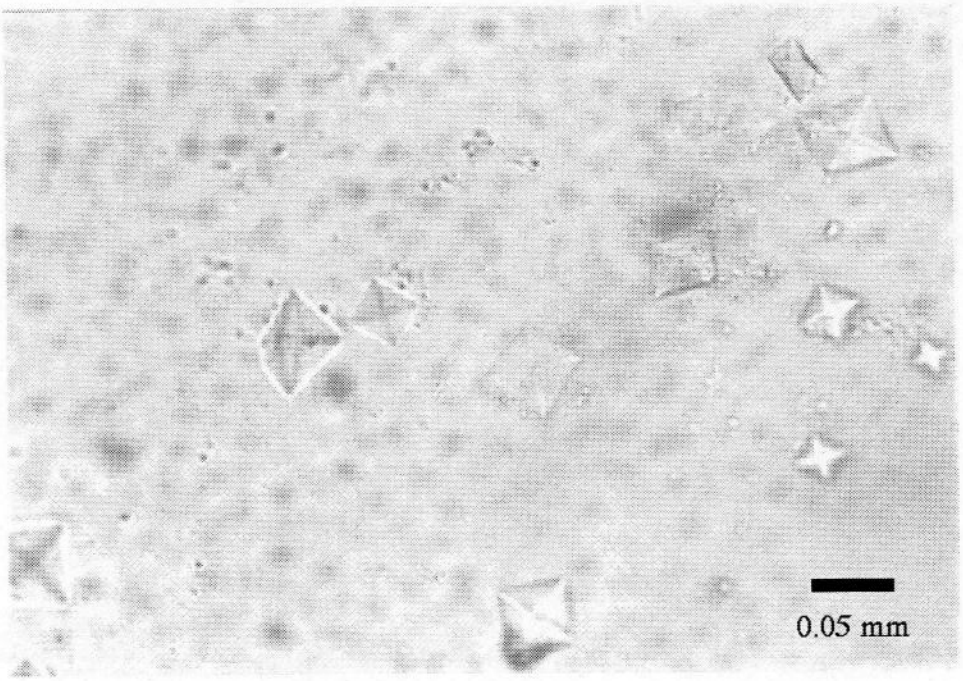

Figure 4-7. Tetragonal bi-pyramidal crystals obtained from Pyrococcus furiosus 70S ribosome preparation with MPD as a precipitant.

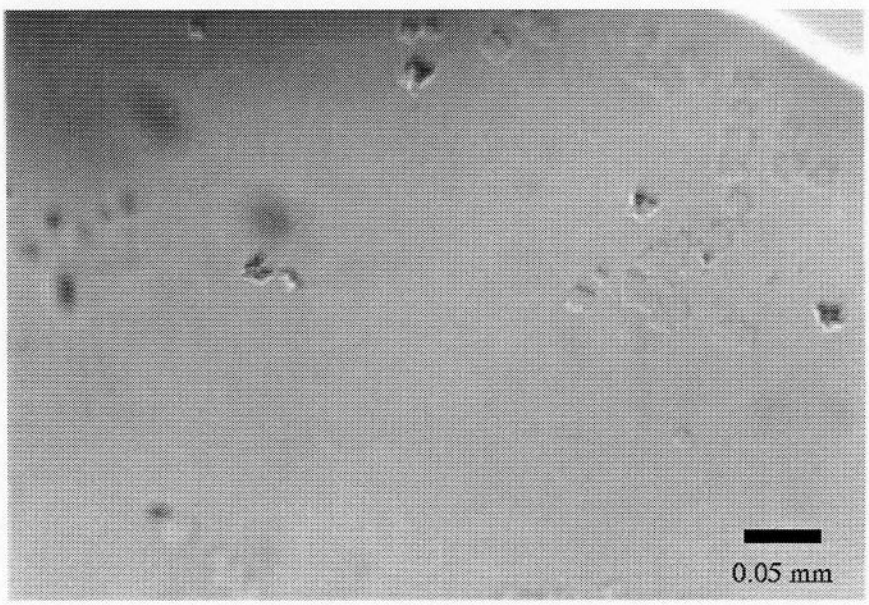

Figure 4-8. Tetragonal bi-pyramidal crystals obtained from Pyrococcus furiosus 70S ribosome preparation with PEG-1000 as a precipitant.

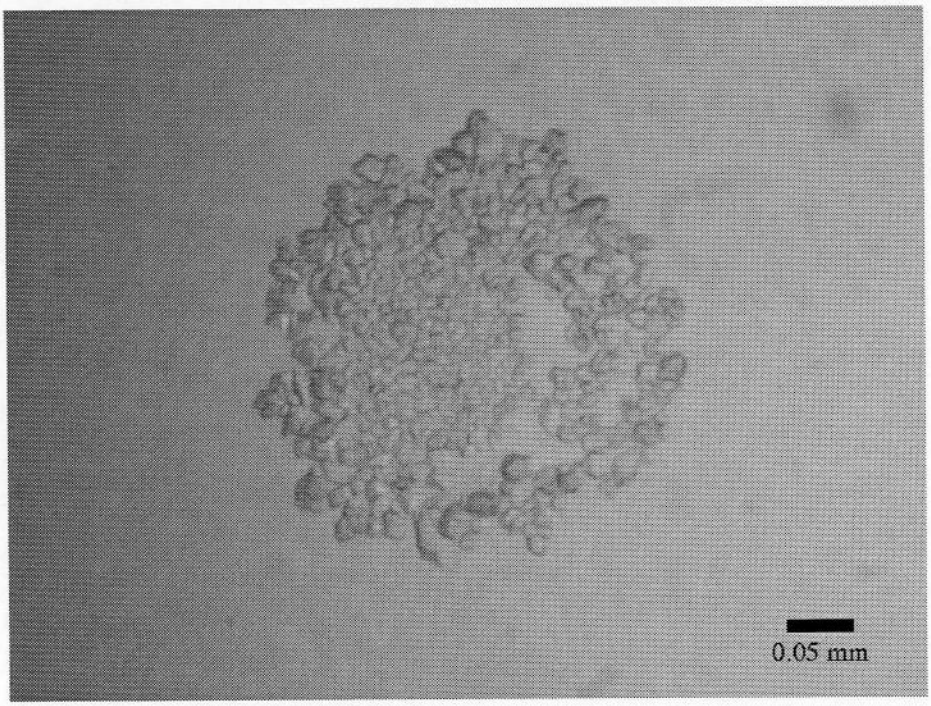

Figure 4-9. The diamond shape crystals from PEG-4000.

experiments were tried to grow crystals bigger.

4-4-2 Re-crystallization

The re-crystallization method is one of the most popular methods to grow crystals bigger. Small crystals from MPD at 25 °C were incubated at 40 ~ 60 °C and they were dissolved. Temperature was then dropped by 1 °C per day until it reached to 25 °C.

4-4-3 Temperature control

The temperature control was tried to get bigger crystals. The crystals by MPD were stored at 30 °C. Then, the temperature was dropped by 1 °C per day until it reached 25 °C to grow crystals slowly.

4-4-4 Dialysis of sample before crystallization

The protein solution was usually mixed with same volume of precipitant (reservoir solution). When the concentration of precipitant was very high, small crystals grew in the solution. Since mixture of sample and reservoir solution produced too many nuclei of crystals. In order to decrease the number of crystal nuclei, the protein

sample used for crystallization was dialyzed against 0.5 %(v/v) MPD buffer before it was equilibrated by the hanging drop vapor diffusion method. The protein sample containing 0.5 % (w/v) MPD was placed on a cover glass, and precipitant solution in the well was covered with it. They were incubated at 25 °C.

4-4-5 Pre-incubation

The 70S ribosome from *Pyrococcus furiosus* have the highest activity at the 60 ~ 98 °C. In order to crystallize active form ribosome, the 70S ribosome sample was incubated at 60 °C just before the crystallization.

4-4-6 Addition of salt to the reservoir solution

The volume of drop is usually decreased with the progress of equilibrium between the drop and reservoir solution. The concentrations of protein and precipitant in the drop increase gradually and crystals grow. However, the vapor diffusion equilibrium of the 70S ribosome preparation was different from the general case. Drop volume increased during equilibrium because of high hydration of 70S ribosome. Increase of drop volume prevented crystals from growing. When crystals were grown

from PEG-4000 solution, they were dissolved after 1 week because the increase of drop volume reduced the concentrations of the ribosome and the precipitant. Thus the NaCl was added to the reservoir solution to regulate the drop volume. In this study, NaCl concentrations were varied from 100 mM to 500 mM in 100 mM steps to control the volume of drops.

4-5 Results

Although the crystals from MPD were incubated at three temperatures of 40 °C, 50 °C and 60 °C, the crystals were not dissolved in any cases. Thus the re-crystallization method could not applied for the present crystallization.

The crystals obtained by this temperature control method were bigger than the crystals obtained in the previous condition. They grew up to 0.15 mm x 0.15 mm x 0.03 mm in 1 week.

Dialysis of sample before crystallization was the most effective method to get larger crystals. The crystals grew up to 0.2 mm x 0.2 mm x 0.04 mm at 25 °C in 1 week.

Pre-incubation was also effective in getting larger crystals. The crystals grew up to 0.2 mm x 0.2 mm x 0.04 mm at 25 °C in 1 week.

The crystals appeared once when the ribosome solution was equilibrated with reservoir solution containing 100 mM NaCl, and they were dissolved later. When 200 mM NaCl was applied for the salt condition of reservoir solution, crystals were stable for long time. In the other conditions (300 mM, 400 mM and 500 mM NaCl was added), the ribosome was precipitated and crystals were not able to grow.

4-6 Optimized conditions for crystallization

Crystallization conditions of were successfully refined. The best crystallization conditions are given in the following descriptions. All the optimized crystallization conditions are given in Table 4-4.

4-6-1 Optimized condition (MPD condition)

After the protein samples were dialyzed against 0.5 % (v/v) MPD buffer, it was centrifuged at 10,000 rpm for 15 min using a MRX-150, TMA-2 rotor (TOMY SEIKO Co. Ltd., Japan) to remove precipitants. The supernatant solution was used for crystallization. It was incubated at 60 °C just before the crystallization. The 5 μl of incubated ribosome solution was placed on a cover glass,

Table 4-4. Optimized conditions

a) Optimized crystallization conditions with MPD

Method	Hanging drop
Buffer	20 mM Tris-HCl
pH	7.5
Protein concentration	40 ~ 60 mg/ml
Precipitant	MPD
drop	0.5 % (w/v)
reservoir	16 % (w/v)
Temperature	25 °C

b) Optimized crystallization conditions with PEG-1000

Method	Hanging drop
Buffer	20 mM Tris-HCl
pH	7.5
Protein concentration	40 ~ 60 mg/ml
Precipitant	PEG-1000
drop	0.5 % (v/v)
reservoir	20 % (v/v)
Temperature	25 °C

c) Optimized crystallization conditions with PEG-4000

Method	Hanging drop
Buffer	20 mM Tris-HCl
pH	7.5
Protein concentration	40 ~ 60 mg/ml
Precipitant	PEG-4000
drop	2 % (v/v)
reservoir	8 % (v/v)
Temperature	20 °C

and a well containing 16 %(v/v) MPD buffer was covered with the glass hanging a drop. Then, it was left at 25 °C. Small crystals appeared in 2 days and grew to 0.5 mm x 0.5 mm x 0.1 mm in 1 week (Figure 4-10).

4-6-2 Optimized condition (PEG-1000 condition)

The protein samples were dialyzed against 0.5 % (v/v) PEG-1000 buffer, and it was centrifuged at 10,000 rpm for 15 min using a MRX-150, TMA-2 rotor to remove precipitants. Pre-incubation was carried out at 60 °C just before the crystallization. The 5 μl of incubated ribosome solution was placed on cover glass, and a well containing 20 %(v/v) PEG-1000 buffer was covered with the glass. Then, they were incubated at 25 °C. The crystals grew up to 0.25 mm x 0.25 mm x 0.05 mm in 1 week (Figure 4-11).

4-6-3 Optimized condition (PEG-4000 condition)

Since it was very difficult to prepare the drop containing the ribosome and 2 %(w/v) PEG-4000 by dialysis, the 2.5μl of ribosome solution was mixed with the same volume of precipitant solution (4 %(w/v) PEG-4000) on a cover glass. The 8 % (w/v) PEG-4000 solution containing 200 mM NaCl was filled in the reservoir well, and they

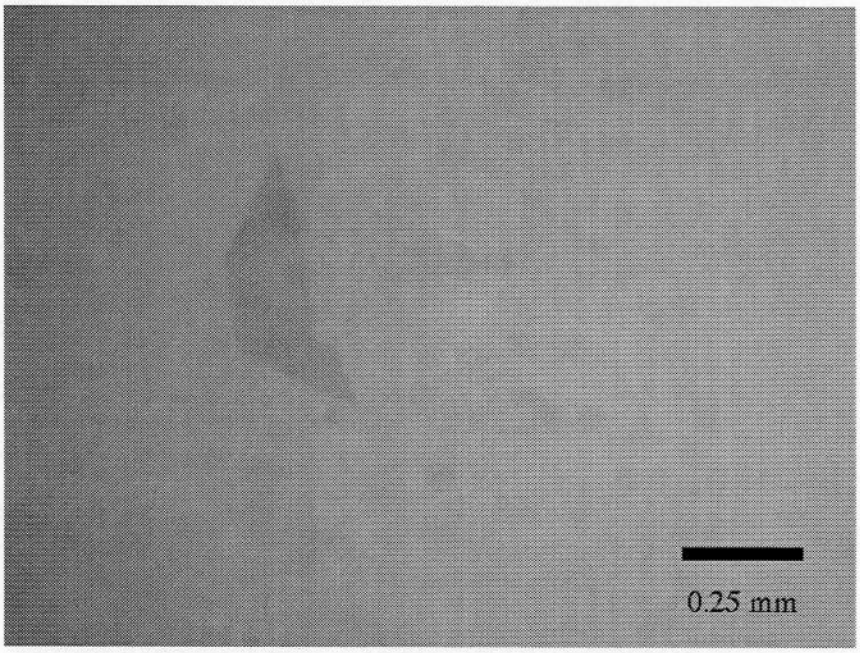

Figure 4-10. Crystals from MPD in optimized condition

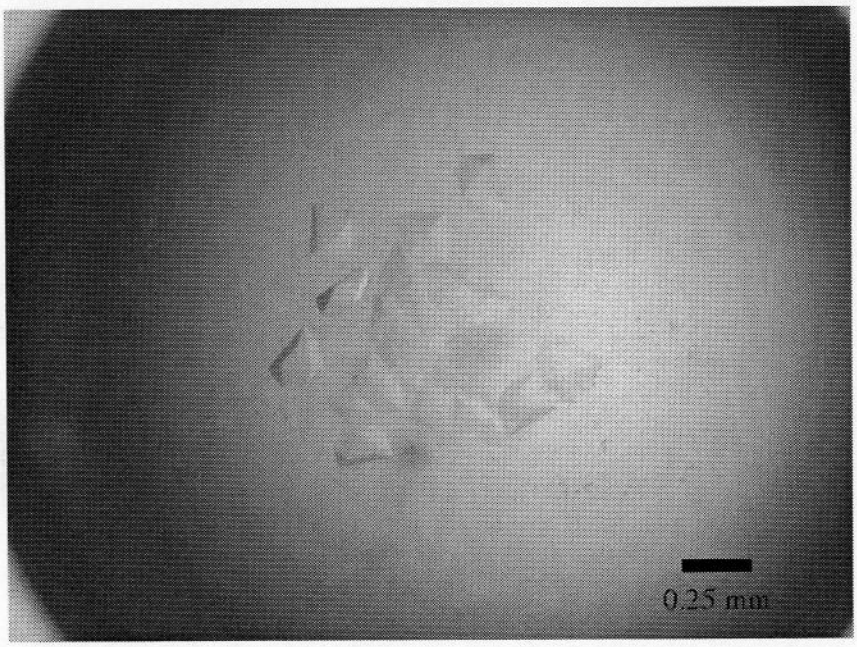

Figure 4-11. Crystals from PEG-1000 in optimized condition

were incubated at 25 °C. Two types of crystals appeared in 2 days. The photographs of crystals were shown in Figure 4-12.

4-7 Component of crystals

Three type crystals were obtained from different conditions. They were collected by centrifugation, and SDS-PAGE and electron microscopy observation were carried out to check the component of these crystals. SDS-PAGE pattern shows existence of 40 KDa main band (Figure 4-13). The electron micrograph of negatively stained sample were shown in Figure 4-14. Large virus like particles with a diameter of about 30 nm were confirmed.

4-8 Crystallization at high temperatures

Crystallization experiments with MPD as a precipitant were also carried out at high temperatures, 60 and 90 °C. The same shape crystals, tetragonal bi-pyramidal crystals, were obtained at both temperatures (Figure 4-15). This results indicated that components of these crystals were thermophilic virus.

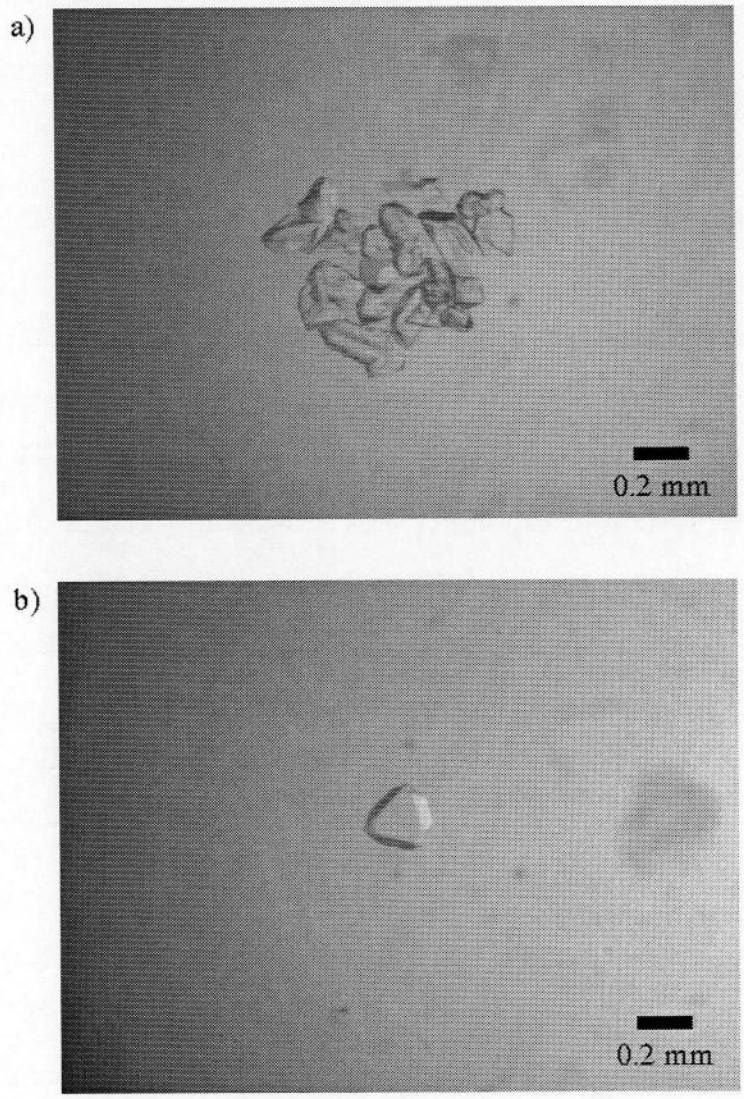

Figure 4-12. Two type crystals from PEG-4000 in optimized condition

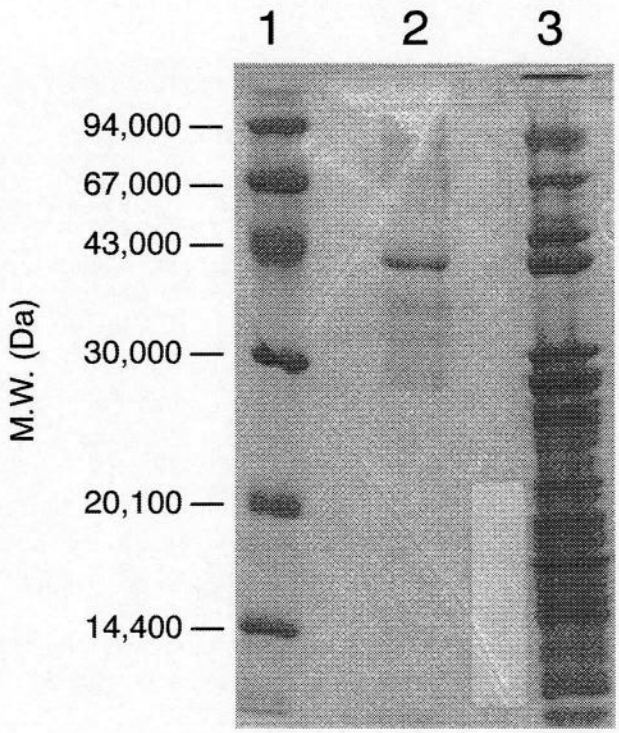

Figure 4-13. SDS-PAGE pattern Lane 1; molecular weight marker, lane 2; crystal and lane 3; ribosome sample.

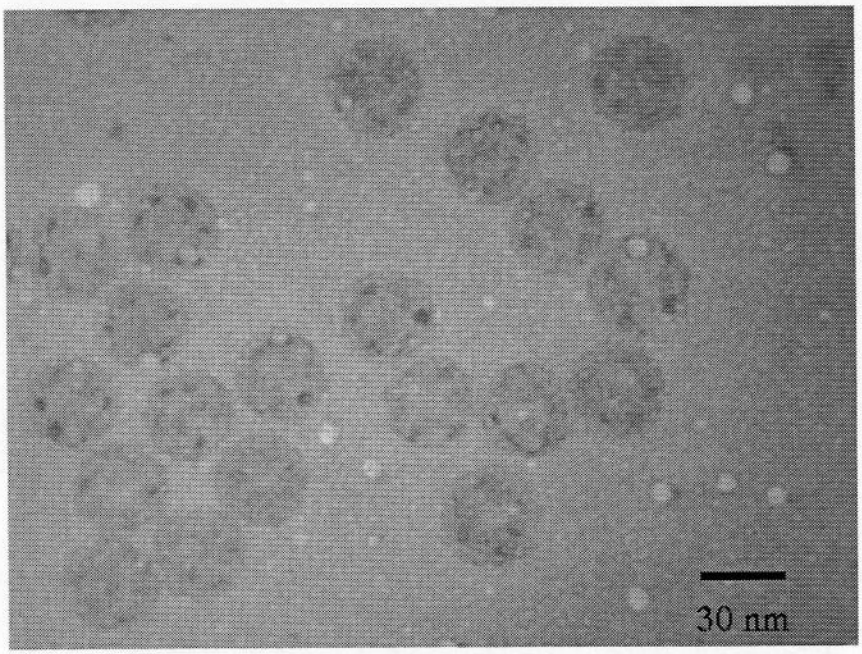

Figure 4-14. Electron micrograph of negatively stained crystal solution. Each particle is about 30 nm in diameter, and has virus like spherical shape.

a) 90 ℃

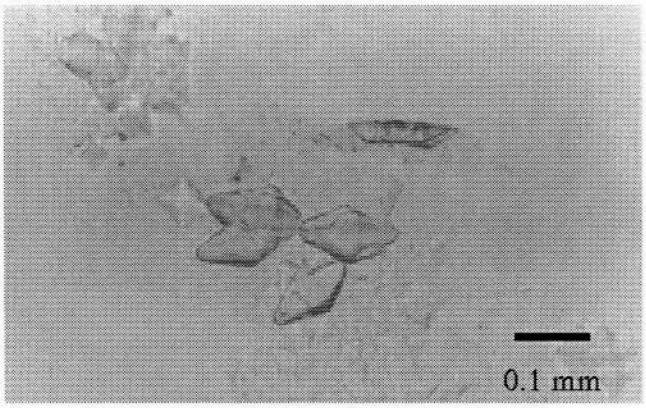

b) 60 ℃

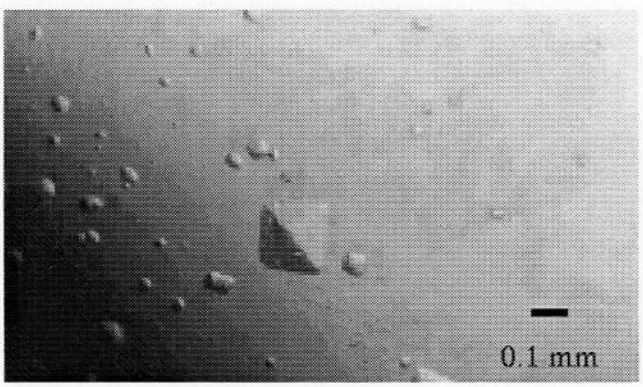

Figure 4-15. Tetragonal bi-pyramidal crystals obtained at a) 60 ˚C and b) 90 ˚C with MPD as a precipitant

Chapter 5

X-ray diffraction experiments

5-1 Introduction

Generally, the crystals of macromolecular assemblies have large unit cell proportional to their molecular weights and diffract X-rays weakly is inversely proportional to their unit cell volume. Since a reciprocal unit cell is inversely proportinal to a unit cell, it is very difficult to separate each diffraction spots of crystals with large unit cell. Use of synchrotron radiation X-rays which are strong and parallel is indispensable for X-ray crystal analysis of the macromolecular assemblies. In 1999, beam line BL44XU for macromolecular assemblies has accomplished in the third generation synchrotron radiation, Super Photon Ring-8 (SPring-8), Hyogo, Japan. This beam line is suitably designed for X-ray diffraction experiment for supramolecular assemblies. All the diffraction experiments were undertaken at the beam line BL44XU of SPring-8, because no diffraction was able to obtain by the laboratory X-ray sources.

5-2 Materials and methods

5-2-1 X-ray diffraction experiments

In this study, X-ray diffraction data were collected by using the image plate detector DIP-2040 (MAC science Co., Ltd., Japan) at the beam line BL44XU. X-ray was monochromatized with Si (1 1 1) monochromator, and focused by a mirror. The wave length of X-rays was tuned at 0.90 Å, and collimated by a collimator a size of 70 μm x 70 μm. The camera length was varied from 500 mm to 1000 mm to separate diffraction spots. All the experimental conditions for X-ray diffraction and crystallographic data are given in Table 5.1 and Table 5.2, respectively.

In the X-ray diffraction experiments by using third generation synchrotron radiation, crystals were damaged by exposure to strong X-rays. The deterioration of crystal lead to decay of X-ray diffraction intensity. Following two causes of the radiation damage of protein crystal are considered.

1) Radicals produced by X-ray irradiation react with proteins in a crystal
2) Rise of temperature by exposure to powerful X-rays

The radiation damage of protein crystal can be reduced by cooling crystal during the data collection. In the

Table 5-1. Experimental conditions for X-ray diffraction of crystals

a) Crystals from MPD

X-ray source	SPring-8 BL44XU
Detector	DIP-2040
Collimator	70 μm
Wavelength	0.9 Å
Camera length	750 mm
Oscillation angle	0.50 °
Overlap	0.00 °
Exposure time	30 seconds
Cryo-protectant	30 %(v/v) MPD
Temperature	100 K

b) Crystals from PEG-4000 and PEG-1000

X-ray source	SPring-8 BL44XU
Detector	DIP-2040
Collimator	70 μm
Wavelength	0.9 Å
Camera length	1000 mm
Oscillation angle	0.50 °
Overlap	0.00 °
Exposure time	30 seconds
Cryo-protectant	30 %(w/v) PEG-4000 or PEG-1000
Temperature	100 K

Table 5-2. Crystallographic data

a) Crystal from MPD

Crystal form	Tetragonal
Space group	$P4_32_12$
Cell constants	$a = b = 633.7$ Å
	$c = 352.5$ Å
Number of molecules in asymmetric unit	Z = 1/2
Volume of asymmetric unit / molecular weight	Vm = 3.05 Å^3/dalton
Solvent content	Vsolv = 59.0 %

b) Crystal from PEG-1000

Crystal form	Tetragonal
Space group	$P4_32_12$
Cell constants	$a = b = 621.9$ Å
	$c = 346.0$ Å
Number of molecules in asymmetric unit	Z = 1/2
Volume of asymmetric unit / molecular weight	Vm = 2.79 Å^3/dalton
Solvent content	Vsolv = 55.9 %

c) Crystal from PEG-4000

Crystal form	Triclinic
Space group	$P1$
Cell constants	$a = b = 340$ Å, $c = 341$ Å
	$\alpha = 120^\circ$, $\beta = 91^\circ$, $\gamma = 117^\circ$
Number of molecules in asymmetric unit	Z = 1
Volume of asymmetric unit / molecular weight	Vm = 2.67 Å^3/dalton
Solvent content	Vsolv = 53.6 %

cryogenic experiment developed by Low *et al.* (1966), crystals are frozen at 100 K with nitrogen steam. Thus, the use of antifreezing solutions (cryo-protectants) is indispensable to prevent nucleation of ice crystals in protein crystals in the course of freezing. Glycerol, ethylene glycol, PEG or MPD are commonly used as cryo-protectants. The cryogenic experiment at 100 K was applied for X-ray data collection. Conveniently, the precipitants used for crystallization in this study, MPD, PEG-1000 and PEG-4000, were available for cryo-protectants, too.

5-2-2 Optimization of condition for cryogenic experiment

Good choice of cryo-protectant can improve dramatically the quality of intensity data, while wrong choice of cryo-protectant seriously deteriorates quality of diffraction data. Thus selection of cryo-protectants is a very important process. In general, cryo-protectants can be chosen from compounds similar to the precipitant in the mother liquors. The same reagents used for the precipitant were available for the cryo-protectant of the resent crystal. The optimum condition of cryo-protectant was searched by varying precipitant concentrations. The 30, 25, 20, 18, 16 %(v/v) MPD solutions were tested as

cryo-protectant for crystals from MPD condition.

5-2-3 Processing of the diffraction data

Diffraction intensities recorded on an imaging plate (IP) were processed with the program DENZO (Otwinowski and Minor, 1997). The intensity of equivalent diffraction spots measured in different IPs were scaled each other and averaged using program SCALEPACK (Otwinowski and Minor, 1997).

5-3 Results

5-3-1 The crystals from MPD

Crystals soaked into 30 %(v/v) MPD solution was frozen by flash-cooling. Cryogenic experiment was carried out under nitrogen gas steam at 100 K. Diffraction images were taken with the IP detector DIP-2040 at BL44XU of SPring-8. X-ray diffraction pattern of a crystal from MPD is shown in Figure 5.1. Although the crystal diffracted up to 6.0 Å, the intensity of spots was decreased sharply beyond 6.5 Å resolution and its mosaicity was high.

5-3-2 The crystals from PEG-1000

Crystals were soaked into 30 %(v/v) PEG-1000 solution. Cryogenic X-ray experiment was carried out as that of the crystal from MPD. X-ray diffraction pattern of a crystal from PEG-1000 is shown in Figure 5.2. The crystal diffracted up to 6.0 Å.

5-3-3 The crystals from PEG-4000

Crystals were soaked into 30 %(v/v) PEG-4000 solution prior to the cryogenic experiment. X-ray diffraction pattern of a crystal from PEG-4000 is shown in Figure 5.3. The crystal diffracted up to 6.0 Å.

5-3-4 Optimization of condition for cryogenic experiment

The optimized cryogenic protectant was 18 %(v/v) MPD solution for a crystal from 16 %(v/v) MPD. In this condition, the high resolution intensity data with very small mosaicity was obtained. The experimental conditions for X-ray diffraction study are summarized in Table 5.7. The best crystal diffracts up to 3.5 Å (Figure 5.4). This resolution of diffraction data is suitable for X-ray crystal structure determination of virus like particle. The crystallographic data of this crystal are given in Table 5.8.

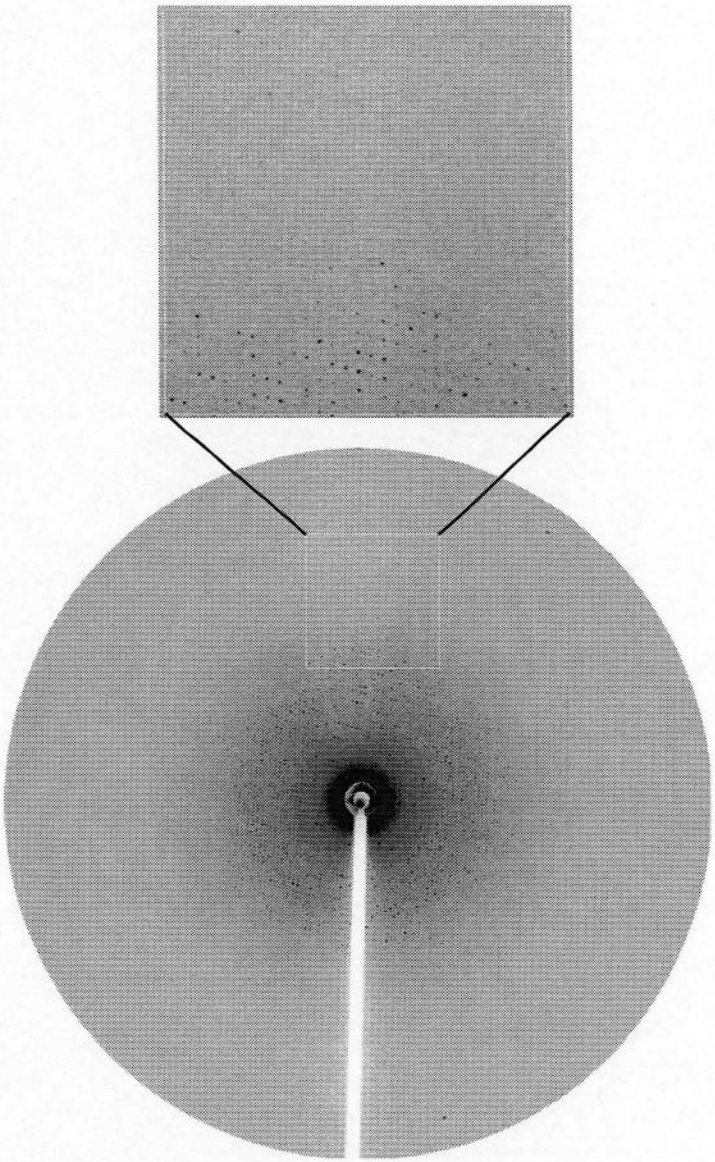

Figure 5-1. X-ray diffraction pattern of crystal from MPD.

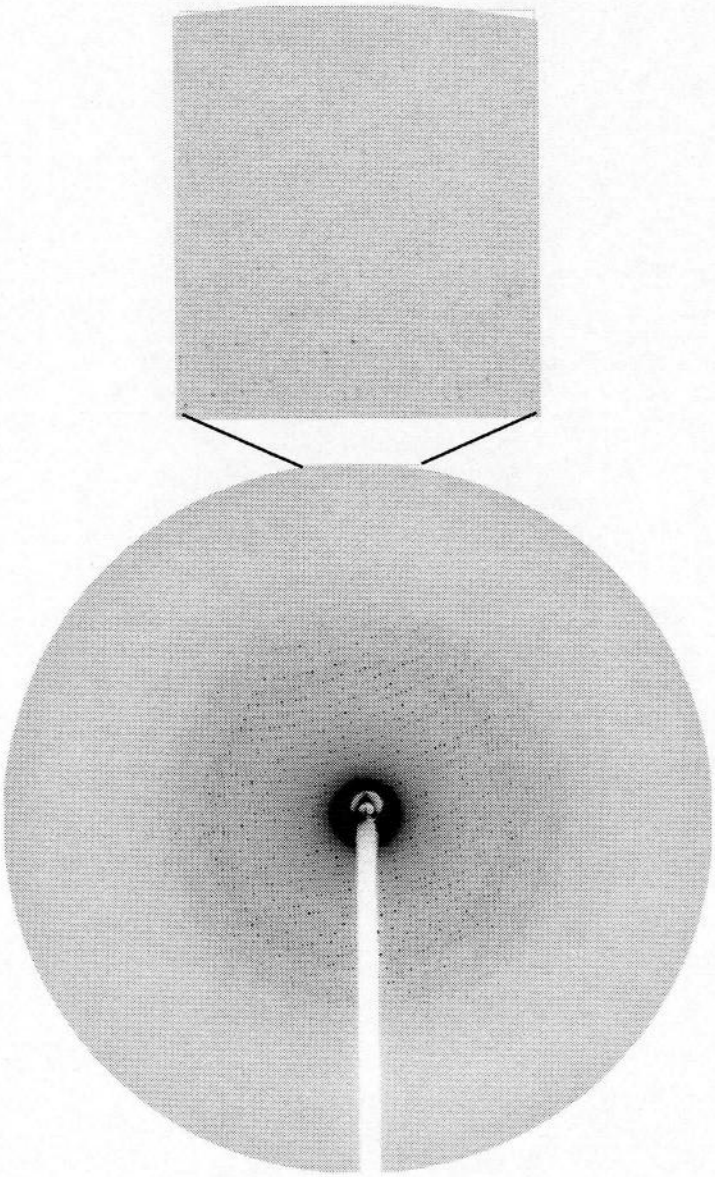

Figure 5-2. X-ray diffraction pattern of crystal from PEG-1000.

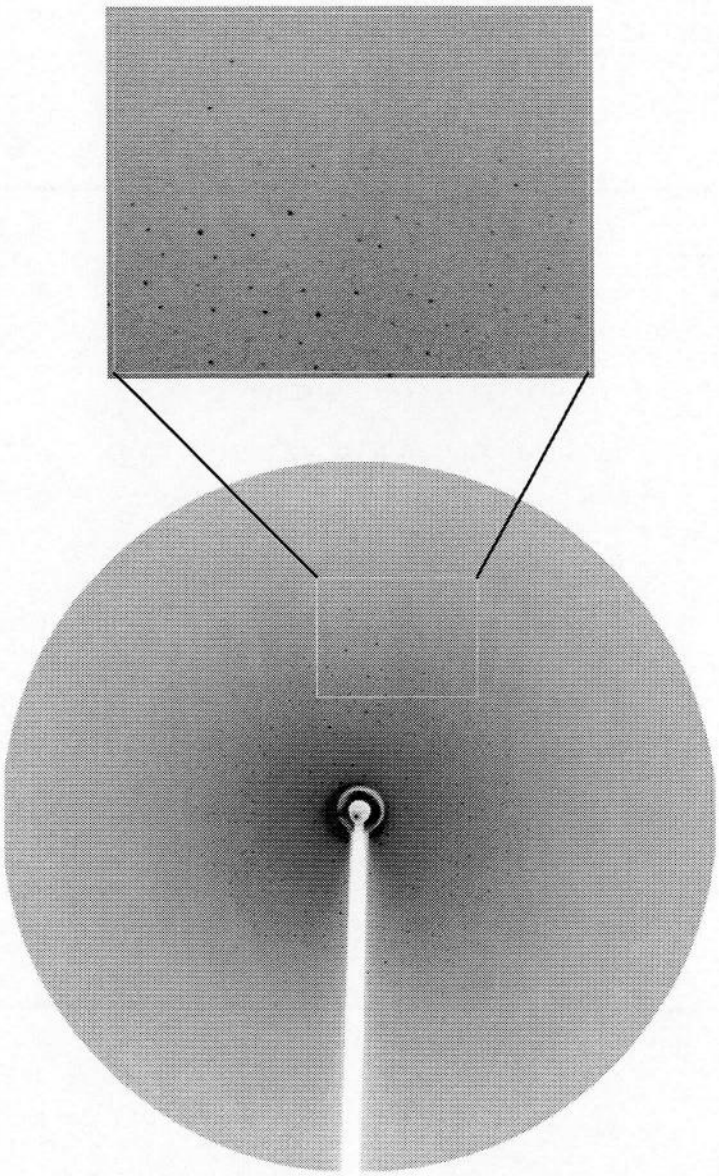

Figure 5-3. X-ray diffraction pattern of crystal from PEG-4000.

Table 5-3. Experimental conditions for X-ray diffraction of crystals from MPD

X-ray source	SPring-8 BL44XU
Detector	DIP-2040
Collimator	70 μm
Wavelength	0.9 Å
Camera length	750 mm
Oscillation angle	0.30 °
Overlap	0.00 °
Rotation speed	0.30 ° / minute
Exposure time	30 seconds
Cryo-protectant	18 %(v/v) MPD
Temperature	100 K

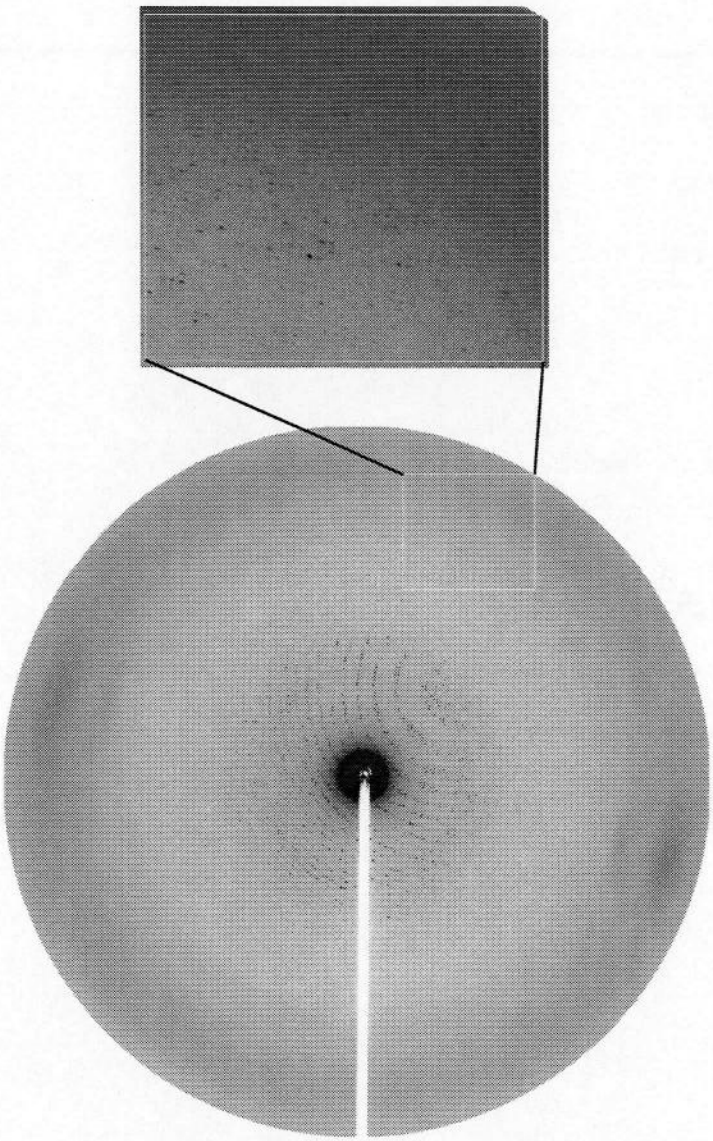

Figure 5-4. X-ray diffraction pattern of crystal from MPD. The condition for cryogenic experiment was optimized. The best crystal diffracts up to 3.5 Å.

Table 5-4. Crystallographic data of crystal from MPD

Crystal form	Tetragonal
Space group	$P4_32_12$
Cell constants	a = 633.7 Å
	b = 633.7 Å
	c = 352.5 Å
Number of molecules In asymmetric unit	Z = 1/2
Volume of asymmetric unit / molecular weight	Vm = 3.05 $Å^3$/dalton
Solvent content	Vsolv = 59 %

5-4 Conclusion

The cryogenic experiment is indispensable to reduce deterioration of the crystal by strong X-rays of third generation synchrotron radiation. Thus, the selection of cryo-protectants assuring high quality intensity data is very important. Usually, the cryogenic experiment is not suitable for X-ray diffraction experiments of virus crystal because its crystalline lattice is easily destroyed by freezing. However, cryogenic experiment was performed successfully in this study.

The crystal obtained from 16 %(v/v) MPD diffracted up to 3.5 Å resolution when it was soaked in 18 %(v/v) MPD solution as cryo-protectant, while the same crystals diffracted only up to 6.5 Å resolution, when it was soaked in 30 %(v/v) MPD solution. Although increasing concentration of cryo-protectants can usually prevent nucleation of ice crystals in a protein crystal on freezing, too high MPD concentration damaged the crystal. Concentrations of cryo-protectants for crystals from PEG-1000 and PEG-4000 should be optimized. Addition of other reagents such as glycerol, ethylene glycol or trehalose may reduce radiation damages of crystal, as in the cases of other protein crystals. The crystals obtained from MPD usually diffracted up to 4.0 Å resolution by 30

seconds X-ray exposure. Since crystals were damaged by irradiation of strong X-ray, only five frames of diffraction were taken at the same position of a crystal. X-rays were shot at several positions of a crystal. The oscillation angle must be less than 0.30 ° to collect intensity data without overlapping of spots at high-resolution because crystals of virus like particle have large cell constants. A total of 60 isomorphous crystals or more are necessary to obtain whole data set. Although this work is very hard, producing the larger size crystals makes it easy. Moreover, the use of liquid helium in cryogenic experiments may reduce deterioration of the crystal by X-ray irradiation.

Chapter 6

X-ray experiments and structure determination

6-1 Native data set

The crystals obtained from MPD usually diffracted up to 4.0 Å resolution by 30 seconds X-ray exposure. Since crystals were damaged by irradiation of strong X-ray, only 5-10 frames of diffraction were taken at the same position of a crystal. X-rays were shot at several positions of a crystal. The oscillation angle must be less than 0.30 ° to collect intensity data without overlapping of spots at high-resolution because crystals of virus like particle have large cell constants. A total of 231 crystals were used for native data collection, and 16 isomorphous crystals were used to obtain whole data set. As shown in Table 6-1, a total of 5,931,092 observed reflections with 98.3 % completeness at 3.7 Å resolution were obtained. Merging R was 0.144 for 731,868 independent reflections, and averaged redundancy was 8.1 for the native data set.

6-2 Preparation of heavy atom derivatives

After high-resolution intensity data were collected, their phases should be determined. The most

Table 6-1. Intensity data collection of native crystal.

crystal	16
Number of frame (IP)	549
Resolution range (Å)	100-4.0
Observed reflections	5,931,092 (365,218)
Independent reflections	731,868 (71,272)
$I/\sigma(I)$	11.7 (2.0)
Averaged redundancy*	8.1 (5.1)
Completeness (%)	98.3 (96.5)
R_{merge} (%)**	14.4 (48.5)

*Redundancy is the number of observed reflections for each independent reflection.

**$Rmerge=\Sigma_{hkl}\Sigma_i \mid I_i\ (hkl)-<I(hkl)> \mid / \Sigma_{hkl}\Sigma_i I_i\ (hkl)$

Figures in parentheses are given for the highest resolution shell.

effective method is multiple isomorphous replacement (MIR) method which generally requires at least two kinds of heavy atom derivative crystals. Heavy atom derivatives were prepared by the conventional soaking method.

Many kinds of heavy atom reagents were tested by varying the soaking conditions such as concentration and soaking period. These conditions used are listed in Table 5-5. All the diffraction data for the screening of heavy atom derivatives were collected by using an IP detector DIP-2040 (MAC science Co., Ltd., Japan) at the beam line BL44XU of SPring-8. The crystal to IP distance was 750 – 850 mm and the oscillation angle was set to 0.5 °. The exposure time per one frame is 30 sec. About 10 frames were collected from each derivative crystals, diffraction intensities were processed with the program DENZO (Otwinowski and Minor, 1997) and scaled by the scaling program SCALEPACK (Otwinowski and Minor, 1997). After scaling the intensity data from the native and heavy atom derivatives, the mean R-factor ($R_{iso} = \Sigma \mid F_{PH} - F_P \mid / \Sigma F_P$) were calculated, where F_{PH} and F_P are derivative and the native structure factor amplitudes, respectively. The qualities of the soaked crystals were checked by the comparison of their diffraction intensities. If any changes in diffraction intensities were observed (R_{iso} = 10 – 25 %), the full set data were collected. Intensity

data of derivative crystals were shown in Table 6-2.

6-3 Phase determination

Three derivative data sets were available for phase datermination. At first, the low-resolution X-ray maps (approximately 10 Å) were calculated using initial phases determined by multiple isomorphous replacement (MIR) coupled with anomalous scattering (MIRAS) of heavy atom clusters, SiW_{12} and $.Ta_6Br_{14}$. Heavy atom sites of normal heavy atom, $LuCl_6$, derivatives were located at 10 Å in a difference Fourier map calculated with these initial phases. The heavy atom parameters are refined at higher resolution using MLPHARE (Otwinowski, 1991). Final refined heavy atom parameters were shown in Table 6-3. The phases obtained by MIR methods were refined by solvent flattening (Wang, 1985). Since electron density distribution showed up a spherical shell, non – crystallographic symmetry of heavy atom site were inspected. Consequently, an icosahedral symmetry for heavy atom positions were identified. Electron density map was refined again by the solvent flattening coupled with non-crystallographic symmetry (NCS) averaging (Bricogne, 1974; Schuller, 1996), and electron density map were shown in Figure 6-1. This spherical particle was

Table 6-2. Intensity data of derivative crystals

	SiW_{12}*	Ta_6Br_{14}**	$LuCl_6$
Used crystal	1		1
Number of frame	180	189	300
Resolution (Å)	8.0 (8.29-8.00)	4.5 (4.66-4.50)	4.45 (4.61-4.45)
Observed reflections	314,158 (14,817)	1,217,624 (92,636)	2,100,019 (149,766)
Independent reflections	68,458 (5,518)	353,243 (33,752)	418,184 (40,849)
$I/\sigma(I)$	8.9 (3.5)	6.9 (2.6)	9.6 (3.2)
Averaged redundancy	4.6 (2.7)	3.4 (2.7)	5.0 (3.7)
Completeness (%)	90.2 (73.8)	85.2 (82.2)	97.9 (96.4)
R_{merge} (%)	13.0 (27.8)	14.7 (32.9)	13.1 (30.7)
R_{iso} (%)	16.3	20.4	12.1
Concentration of Heavy atom reagent (mM)	1.0	0.25	0.65
Soaking period (hours)	6.0 (40 hr Back Soak)	1.0 (No Back Soak)	5.5 (No Back Soak)

*SiW_{12} : $SiO_2 \cdot 12WO_3 \cdot 26H_2O$

**Ta_6Br_{14} : $Ta_6Br_{14}(H_2O)4 \cdot 4H_2O$

Table 6-3. Final refinement of heavy atom parameters

	SiW_{12}	Ta_6Br_{14}	$LuCl_6$
Resolution (Å)	70.0-10.0	70.0-7.50	50.0-5.0
R_{cullis}* (centric)	0.52	0.68	0.93
Phasing power **	2.03	1.46	0.53
Number of site	16	42	26

* $R_{cullis} = \Sigma \mid \mid F_{PH} - F_P \mid - F_H(\text{calc}) \mid / \Sigma \mid F_{PH} - F_P \mid$, where F_H(calc) is the calculated heavy atom structure factor. The summation is over the centric reflections only.

**Phasing power is root-mean-square (rms) isomorphous difference divided by rms residual each of closure.

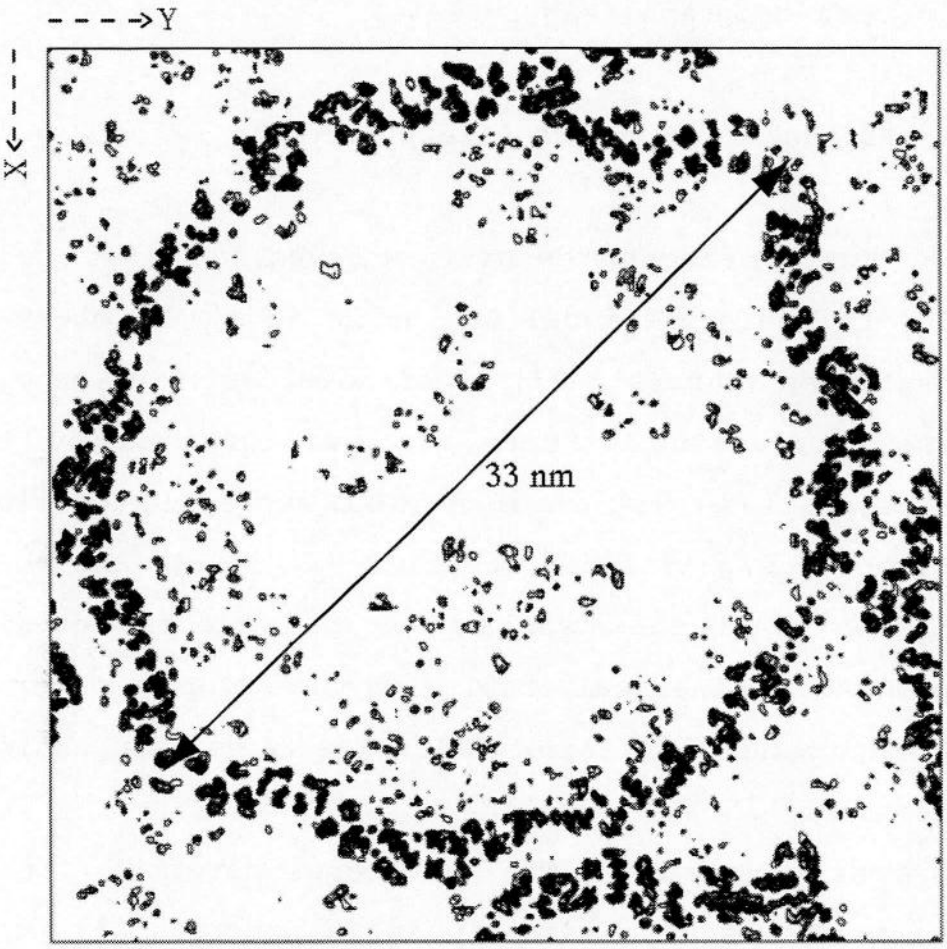

Figure 6-1. Electron density map of virus like particle at 3.8 Å resolution. Section 135/280 ~ 137/280 was shown. The contour level is 1.0 σ. The spherical particle is about 33 nm in diameter with T = 3 icosahedral symmetry.

about 33 nm in diameter with T = 3 icosahedral symmetry, and its shape and size were consistent with results of electron micrograph (Figure 4-14).

6-4 Structure of virus like particle

Current electron density map revealed the main chain fold. Poly alanine model was built into this electron density map (Figure 6-2). After model building of poly alanine, electron density map was improved by the non-crystallographic symmetry (NCS) averaging technique (Bricogne, G., 1974 and Schuller D., 1996), and model building of side chain will be possible. Electron density map showed a spherical shell with the outer diamater of 330 Å and inner diameter of 280 Å. The virus like particle consisting of 180 protein subunits exhibited T = 3 icosahedral symmetry. The structural determination of this supramolecular assembly is in progress at atomic resolution as the first thermophilic virus structure.

a)

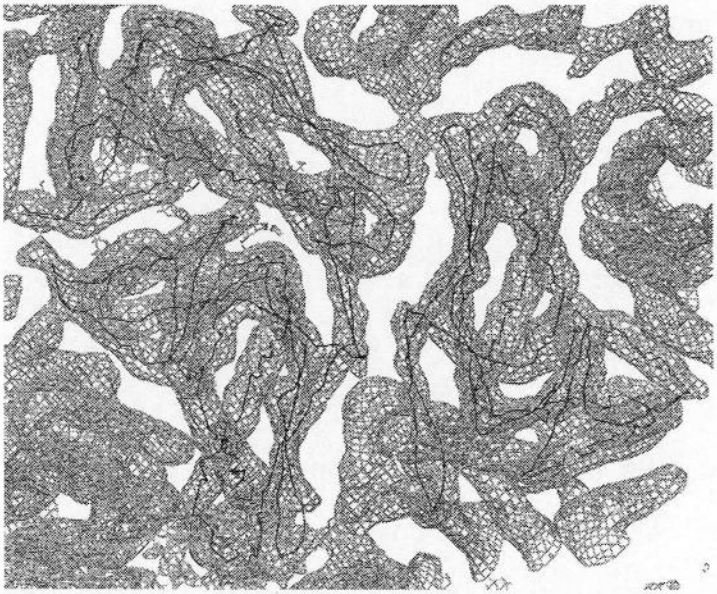

b)

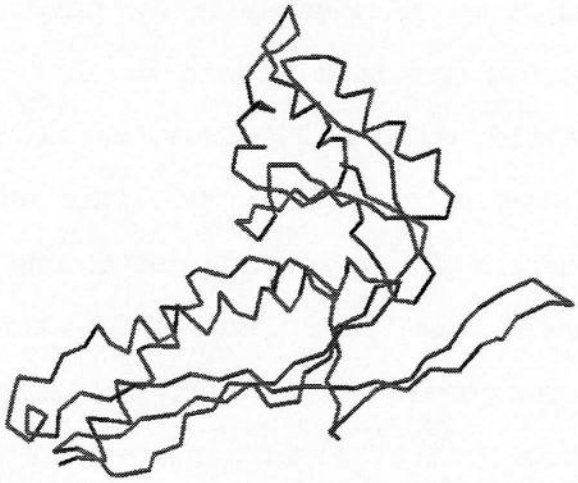

Figure 6-2. Poly alanine model of virus like particle

a) Poly alanine model in 2*Fo-Fc* electron density map

b) Cα -trace of a poly alanine model

Chapter 7

Disscussion

7-1 Thermal stability of *Pf*PCP

The crystal structures of pyrrolidone carboxyl peptidase from *P. furiosus* and its Cys-free mutant were determined at 2.2 and 2.7 Å, respectively. Its extremely high stability was explained on the basis of its and two homologous structures from a hyperthermophile and a mesophile. The high stability of *Pf*PCP was caused by the increases in hydrophobic interaction and hydrogen bonds, the formation of an inter-subunit ion pairs network, and the improvement to an ideal conformation. On the other hand, the stabilization of *Tl*PCP was mainly caused by the remarkable increase in hydrophobic interaction and the decrease in denaturation entropy due to the formation of disulfide bonds. From these results and those previously reported, we can conclude that a hyperthermophile protein does not have any universal factors responsible for their extremely high stability and that the combination of positive and negative factors for stabilization effects in their conformation stability are superior to that of a mesophile protein.

7-2 Application of virus like particle

This virus was the first virus from hyper - thermophilic bacterium. Not only subunit protein of virus but also virus were stable at high temperature. The intact virus particle contains RNA inside the spherical shell. The virus must be able to accommodate various substances inside the spherical shell instead of RNA. This virus particle is a molecular compartment with extremely high thermostability.

The strong medicines such as anticancer agent have serious side effects because they do not act on only target site but also other sites. As a result, the utilities of medicines are remarkably reduced. The Drug Delivery System (DDS) is a new technology, which can carry medicines or genes to the designated site by using liposome or virus as a vector. This technique is attractive as a therapeutic method because they can reduce drug toxicity and can increase drug utility. This spherical particle will be applicable to biological clathrate compound such as DDS. Moreover, the remarkable feature of this particle is that they are stable at high temperature, 95 ~ 100 °C, and it is more stable than any other vectors used for DDS.

7-3 Mechanisms of Crystallization of virus

The crystals of virus like particle were obtained from high concentrated ribosome solution, and they diffracted up to 3.5 Å esolution. Usually, purity of protein sample is the most important factor to obtain its crystal which diffracted X-ray at high resolution. The electron micrograph of negatively stained 70S ribosome solution showed that ratio of virus like particles in 70S ribosome solution was extremely lower than ribosome particles. There has been no report of successful case of crystallization like this. The following is a possible mechanism of crystallization of virus in this study. A few virus particles were included in the 70S ribosome preparation. Since ribosome particle was highly hygroscopic, the 70S ribosome contained in sample solution acted as a precipitant such as polyethylene glycol (PEG). This is consistent with the experimental result that this virus like particle was not crystallized in the purified virus solution containing no ribosome. Consequently, ribosome promotes nucleation of virus particles at low concentration.

7-4 Purification and crystallization of 70S ribosome

The 70S ribosome purification procedure used in this investigation, an improved method of Visentin *et al.*, is unique. For most of protein purification, column chromatography, such as ion exchange chromatography, is very effective technique. However, it cannot be applied for purification of 70S ribosome because the components of 70S ribosome are easily removed during the experiment. Therefore, no column chromatography was used for the purification to avoid removal of ribosomal components. In the present method, the 70S ribosome was successfully purified by the centrifugation, ultra-centrifugation and density gradient centrifugation. Especially, two discontinuous density gradient steps were superior to other recently developed procedures. In the sucrose density gradient step, a lot of various factors were removed completely as a supernatant and ribosome which included tRNA and mRNA were prepared as a precipitate. Second discontinuous density gradient step, glycerol discontinuous density gradient centrifugation, tRNA and mRNA were removed completely as a supernatant and only free 70S ribosome were prepared as a precipitate. Moreover, discontinuous density gradient was more convenient than

continuous one, and pure 70S ribosome was prepared with high yield in a short time. Although this purified sample was used for crystallization, contamination of virus like particle was confirmed in this sample. Therefore, it is necessary to remove virus like particles to crystallize the 70S ribosome. The density gradient centrifugation, gel filtration chromatography and hydrophobic chromatography at the final step of purification will be available for removal of virus like particle. Alternative way of the ribosome purification from *P.furiosus* is to choose a knock out stain for the virus in bacterial gene.

7-5 Conclusion

In the study of thermal stability of *Pf*PCP, the factor of thermal stability was evaluated quantitatively. There is not a universal factor for the thermal stability. Thermal stability of proteins was effected by the combination of various factors, which are different for every proteins.

I succeeded in obtaining the high quality crystals of novel virus like particle from *Pyrococcus furiosus*. This is the first crystal of virus from hyperthermophilic archaebacteria. Its gene was integrated in the *P.furiosus*

gene, and they are not shown in the database of *P. furiosus* gene. The crystals diffracted up to 3.5 Å resolution with a small mosaicity. At this resolution, it is possible to built coat protein models. When mechanism of thermotolerance of thermophilic virus is elucidated, this hyperthermophilic spherical particle will be applicable to biological clathrate compound.

X-ray crystallography is the most powerful method to obtain a reliable molecular structure. The techniques of X-ray crystallographic analysis have been improved in both hardware and software. Time required for structural determination has been shortened, while the techniques for crystallizing proteins have not been established. Crystallization process is usually the most time consuming in the X-ray crystallographic analysis of a protein. Since ribosome is a supramolecular assembly composed of a lot of components including RNA, crystallization of whole particle is much more difficult than that of a protein. The 70S ribosome was purified with high activity and homogeneity in this study. However only a few amount of contamination of virus particle was prevents the 70S ribosome from crystallizing. Removal of this particle makes it possible to crystallize the 70S ribosome.

Refernces

Aguilar, C.F., Sanderson, I., Moracci, M., Ciaramella, M., Nucci, R., Rossi, M., and Pearl, L.H. (1997) *J. Mol. Biol.* **271**, 789-802.

Barlow, D.J. and Thornton, J.M. (1983) *J. Mol. Biol.* **168**, 867-885.

Bricogne, G. (1974) *Acta Cryst.* **A30**, 395-405.

Britton, K.L., Baker, P.J., Borges, K.M., Engel, P.C., Pasquo, A., Rice, D.W., Robb, F.T., Scandurra, R., Stillman, T.J., and Yip, K.S. (1995) *Eur. J. Biochem.* **229**, 688-695.

Brunger, A.T. (1987) Yale University Press, New Haven and London

Brunger, A.T., Adams, P.D., Clore, G.M., Delano, W.L., Gros, P., Grosse-Kunstleve, R.W., Jiang, J.S., Kuszewski, J., Nilges, M., Pannu, N.S., Read, R.J., Rice, L.M., Simonson, T., and Warren, G.L. (1998) *Acta Cryst.* **D54**, 905-921.

Collaborative Computational Project, Number 4 (1994) The CCP4 suite: programs for protein crystallography. *Acta Cryst.* **D50**, 760-763.

Connolly, M.L. (1993) *J. Mol. Graph.* **11**, 139-141.

Dams, T. and Jaenicke, R. (1999) *Biochemistry* **38**, 9169-9178.

Eriksson, A.E., Baase, W.A., Zhang, X.-J., Heinz, D.W., Blaber, M., Baldwin, E.P., and Matthews, B.W. (1992) *Science* **255**, 178-183.

Funahashi, J., Takano, K., Yamagata, Y., and Yutani, K. (1999) *Protein Eng.* **12**, 841-850.

Funahashi, J., Takano, K., and Yutani, K. (2001) *Protein Eng.* **14**, 127-134.

Hening, M., Darimont, B., Sterner, R., Kirschner, K., and Jansonius, J.N. (1995) *Structure* **3**, 1295-1306.

Hening, M., Sterner, R., Kirschner, K., and Jansonius, J.N. (1997) *Biochemistry* **36**, 6009-6016.

Hess, D., Kruger, K., Knappik, A., Palm, P., and Hensel, R. (1995) *Eur. J. Biochem.* **233**, 227-237.

Jaenicke, R. and Bohm, G. (1998) *Curr. Opin. Struct. Biol.* **8**, 738-748.

Jaenicke, R., Schurig, H., Beaucamp, N., and Ostendorp, R. (1996) *Adv. Protein Chem.* **48**, 181-269.

Jiang, J.-S. and Brünger, A.T. (1994) *J. Mol. Biol.* **243**, 100-115.

Jones, T.A. (1985) *Methods in Enzymology* (Carter Jr., C.W. and Sweet, R.W., eds.) Vol. 115, pp. 157-171, Academic Press, New York

Jones, T.A., Zou, J.Y., Cowan, S.W., and Kjeldgaard, M. (1991) *Acta Cryst.* **A47**, 110-119.

Kauzmann, W. (1959) *Adv. Protein Chem.* **14**, 1-63.

Knapp, S., Karshikoff, A., Berndt, K.D., Christova, P., Atansov, B., and Ladenstein, R. (1996) *J. Mol. Biol.* **264**, 1132-1144.

Knapp, S., de Vos, W.M., Rice, D., and Ladenstein, R. (1997) *J. Mol. Biol.* **267**, 916-932.

Korndorfer, I., Steipe, B., Huber, R., Tomschy, A., and Jaenicke, R. (1995) *J. Mol. Biol.* **246**, 511-521.

Kraulis, P.J. (1991) *J. Appl. Cryst.* **24**, 946-950.

McCrary, B.S., Edomondson, S.P., and Shriver, J.W. (1996) *J. Mol. Biol.* **264**, 784-805.

Odagaki, Y., Hayashi, A., Okada, K., Hirotsu, K., Kabashima, T., Ito, K., Yoshimoto, T., Tsuru, D., Sato, M., and Clardy, J. (1999) *Structure* **7**, 399-411.

Ogasahara, K., Khechinashvili, N.N., Nakamura, M., Yoshimoto, T., and Yutani, K. (2001) *Eur. J. Biochem.* **268**, 3233-3242.

Ogasahara, K., Nakamura, M., Nakura, S., Tsunasawa, S., Kato, I., Yoshimoto, T., and Yutani, K. (1998) *Biochemistry* **37**, 17537-17544.

Oobatake, M. and Ooi, T. (1993) *Prog. Biophys. Mol. Biol.* **59**, 237-284.

Ota, M., Kanaya, S., and Nishikawa, K. (1995) *J. Mol. Biol.* **248**, 733-738.

Otwinowski, Z. (1991) Daresbury Study Weekend proceedings.

Otwinowski, Z. and Minor, W. (1997) *Methods in Enzymology* (Carter Jr., C.W. and Sweet, R.W., eds.) Vol. 276, pp. 307-326, Academic Press, New York

Pace, C.N., Shirley, B.A., McNutt, M., and Gajiwala, K. (1996) *FASEB J.* **10**, 75-83.

Pappenberger, G., Schurig, H., and Jaenicke, R. (1997) *J. Mol. Biol.* **274**, 676-683.

Roman A Laskowski, Malcolm W MacArthur, David S Moss and Janet M Thornton (1993) *J. App. Cryst.* **26** 283.

Russell, R.J.M., Ferguson, J.M.C., Hough, D.W., Danson, M.J., and Taylor, G.L. (1997) *Biochemistry* **36**, 9983-9994.

Russell, R.J.M., Hough, D.W., Danson, M.J., and Taylor, G.L. (1994) *Structure* **2**, 1157-1167.

Schuller, D. (1996) *Acta Cryst.* **D52**, 425-434.

Schumann, J., Bohm, G., Schumacher, G., Rudolph, R., and Jaenicke, R. (1993) *Protein Sci.* **12**, 1612-1620.

Singleton, M.R., Isupov, M.N., and Littlechild, J.A. (1999) *Structure* **7**, 237-244.

Spassov, V.Z., Karshikoff, A.D., and Ladenstein, R. (1995) *Protein Sci.* **4**, 1516-1527.

Sterner, R., Kleemann, G.R., Szadkowski, H., Lustig, A., Hennig, M., and Kirschner, K. (1996) *Protein Sci.* **5**, 2000-2008.

Tahirov, T.H., Oki, H., Tsukihara, T., Ogasahara, K., Yutani, K., Ogata, K., Izu, Y., Tsunasawa, S., and Kato, I. (1998) *J. Mol. Biol.* **284**, 101-124.

Takano, K., Ota, M., Ogasahara, K., Yamagata, Y., Nishikawa, K., and Yutani, K. (1999) *Protein Eng.* **12**, 663-672.

Takano, K., Yamagata, Y., Funahashi, J., Hioki, Y., Kuramitsu, S., and Yutani, K. (1999) *Biochemistry* **38**,

12698-12708.

Takano, K., Yamagata, Y., and Yutani, K. (1998*J. Mol. Biol.* **280**, 749-761.

Tanner, J., Hecht, R.M., and Krause, K.L. (1996) *Biochemistry* **35**, 2597-2609.

Villeret, V., Clantin, B., Tricot, C., Legrain, C., Roovers, M., Stalon, V., Glansdorff, N., and Van Beeumen, J. (1998) *Proc. Natl. Acad. Sci. USA* **95**, 2801-2806.

Wang, B.C. (1985) *Methods Enzymol.* **115**, 90-112.

Yamagata, Y., Ogasahara, K., Hioki, Y., Lee, S.J., Nakagawa, A., Nakamura, H., Ishida, M., Kuramitsu, S., and Yutani, K. (2001) *J. Biol. Chem.* **276**, 11062-11071.

Yip, K.S.P., Stillman, T.J., Britton, K.L., Artymiuk, P.J., Baker, P.J., Sedelnikova, S.E., Engel, P.C., Pasquo, A., Chiaraluce, R., and Consalvi, V. (1995) *Structure* **3**, 1147-1158.

Zhang, K.Y.J. and Main, P. (1990) *Acta Cryst.* **A46**, 377-381.

List of publications

X-Ray Crystalline Structures of Pyrrolidone Carboxyl Peptidase from a Hyperthermophile, *Pyrococcus furiosus*, and Its Cys-Free Mutant
Hideaki Tanaka, Masanobu Chinami, Tsunehiro Mizushima, Kyoko Ogasahara, Motonori Ota, Tomitake Tsukihara, and Katsuhide Yutani
J. Biochem. Vol. 130, pp. 107-118 (2001)

Crystallization of novel virus from Hyperthermophile, *Pyrococcus furiosus*.
Hideaki Tanaka, Eiki Yamashita, Khoon Tee CHONG, Naohiro MATSUGAKI, Yuichiro NAKAISHI, Masanao MICHINOMAE, Masahiro URITANI, Masaki YAMAMOTO, Yoshizumi ISHINO, Atsushi NAKAGAWA and Tomitake TSUKIHARA
in preparation